

Facies Analysis, Sequence Development and Paleoredox Condition of Lower Part of Kaimur Formation, Vindhyan Supergroup, Central India

**Thesis submitted for the partial fulfillment of the Msc. Degree in
Applied Geology of Jadavpur University**

Submitted by

ADITI BISWAS

Examination roll no. MGEO194029

Registration No. 142789 of 2017-18

Under the supervision of

Prof. SUBIR SARKAR

Department of Geological Sciences

Jadavpur University

Kolkata-700032

2019

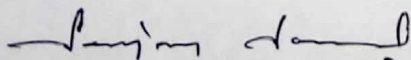


CERTIFICATE

This is to certify that Ms. **ADITI BISWAS** of M.Sc. Final Year, 2019, bearing examination Roll No. **MGEO194029** and Registration No **142789 of 2017-18**, has worked under my guidance in the Department of Geological Sciences and completed her thesis entitled “**FACIES ANALYSIS, SEQUENCE DEVELOPMENT AND PALEOREDOX CONDITION OF LOWER PART OF KAIMUR FORMATION, VINDHYAN SUPERGROUP, CENTRAL INDIA**” which is being submitted towards partial fulfilment of her M.Sc. Final Examination in Applied Geology of Jadavpur University in 2019.

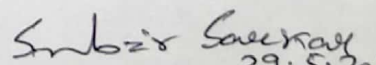
Date: 29.05.2019

Place: Kolkata


29.5.19
PROF. SANJOY SANYAL

(HEAD OF THE DEPARTMENT)

Head
Department of Geological Sciences
Jadavpur University
Kolkata-700032


29.5.2019
PROF. SUBIR SARKAR

(SUPERVISOR)

Dr. Subir Sarkar
Professor
Department of Geological Sciences
Jadavpur University
Kolkata - 700 032

Acknowledgement

I would like to express my heartfelt gratitude and deepest appreciation to my guide **Prof. Subir Sarkar**. He continuously makes efforts to inculcate an appreciation towards science and research through his teachings. His knowledge, expertise, critical comments and guidance were pivotal in the completion of this dissertation work.

I would like to thank **Dr. Soumik Mukhopadhyay** and **Dr. Sunipa Mandal** for their continuous support and guidance throughout the course of this dissertation.

I am deeply indebted to all the members of the Sedimentological Laboratory at the Dept. Of Geological Sciences, Jadavpur University. I would like to thank **Mr. Sabyasachi Mandal**, **Dr. Adrita Choudhuri**, **Ms. Indrani Mandal**, **Ms. Susmita Sarkar**.

My dissertation would not have been completed without the continuous guidance of **Mr. Sabyasachi Mandal**.

I am deeply thankful to all the people connected directly or indirectly in the completion of this dissertation work.

Finally, I am grateful to my parents for their continuous support and encouragement.

Date: 31.05.2019

Aditi Biswas.
(ADITI BISWAS)

Abstract

The Sandstone present above the Rohtas Limestone and the overlying Bhagwar shale have been studied during the present work. Below the sandstone there is a transgressive lag which indicate a fresh start of sedimentation after the completion of deposition of Rohtas limestone. The sandstone is likely to be the equivalent of lower quartzite member and consists of two associations. Detailed sedimentological investigation suggests that it is basically a tide dominated deposit with some intervention of storms. The sandstone is followed by a shale deposits which is black in colour. Considering the detailed sedimentology and sequence stratigraphy it is likely that deposition initiated on the unconformity surface present above the Rohtas limestone followed by a transgressive system tract(TST) and the maximum flooding surface. In this transgressive sequence a glaucony horizon has been identified. The glaucony minerals are rich in Mg and K₂O content.

TABLE OF CONTENTS

| | Page No. |
|---|-----------------|
| Chapter 1: Introduction _____ | 1 |
| Chapter 2: Facies analysis and depositional environment _____ | 17 |
| <i>2.1. Facies distribution of thick sandstone unit above Rohtas Limestone</i> _____ | 18 |
| <i>2.2. Facies distribution of silt (fine) and shale (black) Alternations</i> _____ | 27 |
| <i>2.3. Facies distribution of “siltstone succession” above alternating “fine silt and black shale deposit”</i> _____ | 30 |
| <i>2.4 Facies distribution of thick grey to black shale deposit</i> _____ | 33 |
| Chapter 3: Geochemical analysis of Glaucony on top most horizon of Lower quartzite _____ | 37 |
| Chapter 4: Sequence building pattern of lower part of Kaimur formation _____ | 55 |
| Chapter 5: Discussion and conclusion _____ | 60 |
| References _____ | 64 |

Chapter 1

Introduction

The paleo to Mesoproterozoic Vindhyan Supergroup , largest ‘Purana’ basin in India and World’s second largest Proterozoic basin, is one of the most well studied and focused proterozoic succession in India(Auden 1933;Banerjee 1974; Sastry and Moitry 1984; Bhattacharyya 1996; Seilacher et al. 1998; Bose et al. 2001,2015; Ray et al. 2002; Rusmussen et. al. 2002; Sarkar et. al. 2002a, 2004,2006, 2014; Banerjee et al. 2006; Malone et al. 2008; Bengtson et. al. 2009,2017;Kumar and Sharma 2011; Chakraborty et al. 2012; Bickford et. al. 2018; Gilleaudeau et al. 2018; Mishra et al. 2018; Sallstedt et al. 2018). The Vindhyan rocks are well exposed in Bihar, Uttarpradesh, and Madhhyapradesh while other parts are exposed in Rajasthan area (Chakaraborty, 2002). The vindhyansupergroup comprises a succession of sandstone, shale and limestone/ dolomite with horizon of volcanoclastic sediment (porcellanite) particularly in lower part (Bose et al., 2001). The Son valley Vindhyan sediment succession has two distinct subdivision separated by an unconformity (Sarkar et al; 1996) i.e. lower Vindhyan/ Semri Group and upper Vindhyan. The lower Vindhyan consists of five formations while the upper one consists of three formations (Fig. 1.1; Bose et al. 2001). Though the position of unconformity is well established but the exact stratigraphic position of the unconformity is still controversial.

Though the position of unconformity is well established but the exact stratigraphic position of the unconformity is still controversial.

The lower Vindhyan/ Semri Group which comprises of five formations like Deoland , Kajrahat, Porcellanite, Khenjua, and Rohtas and upper Vindhyan contains three formations like Kaimur, Rewa and Bhandar formation. All the formations are significantly different from each other by lithofacies, depositional environment, records of volcanism, lateral variation in facies thickness and scale of syndepositional deformation features between the two divisions (Chakraborty, 1995; Bose et al., 1997,2001, Sarkar et al., 2002).

This present dissertation is based on the detailed facies analysis, Sequence development and depositional environment in lower part of Kaimur Formation of Vindhyan supergroup.

| Group | Fm. | Member | Description | Paleogeography |
|--|--------------------------------------|--|----------------------------|-------------------------------------|
| V I N D H Y A N S U P E R G R O U P | U P P E R | B H A N D E R | Upper Bhandar Sandstone | Fluvio-eolian and marginally marine |
| | | | Sirbu Shale | Shelf Lagoon |
| | | | Lower Bhandar Sandstone | Coastal playa |
| | | | Bhandar Limestone | Shallow marine |
| | | | Ganuragarh Shale | Chenier |
| | V I N D H Y A N | R E W A | Rewa sandstone | Tidal to fluvio-eolian |
| | | | Rewa Shale | Shelf |
| | K A I M U R | | Dhandraul Sst. | Shelf in fluvio-eolian |
| | | | Scarp Sst. | |
| | | | Bijaigarh Sh. | Intertidal to Shelf |
| | | | Upper Quartzite | |
| | | | Silicified Sh./Bhagwar Sh. | |
| | | | Sasaram Sst. (LQ) | |
| | L O W E R | R O H T A S | Rohtas Limestone | Shelf |
| | | | Rampur Shale | Shelf |
| | | K H E - I N J U A | Chorhat Sandstone | Shallow marine |
| | | | Koldaha Shale | Dominantly shalf, deltatic fluvial |
| | | | PORCELLANITE | Shallow marine |
| | V I N D H Y A N | K A J H R - A H A T | Kajrahat Limestone | Subtidal to peritidal |
| | | | Arangi Shale | Shelf |
| | | D E O - L A N D | | Shallow Shelf |

Fig. 1.1.Stratigraphy of Vindhyan Supergroup and its depositional environment (Bose et al., 2001)

1.1 Area of study:

The investigated area is in and around Kymore in the district of Satna, Madhya Pradesh provides a good section which gives rise to enormous amounts of sedimentary features and structural elements (Figure 1.2). Kymore is situated about 1000km away from Kolkata and is well connected by rail from Allahabad and Katni through broad gauge.

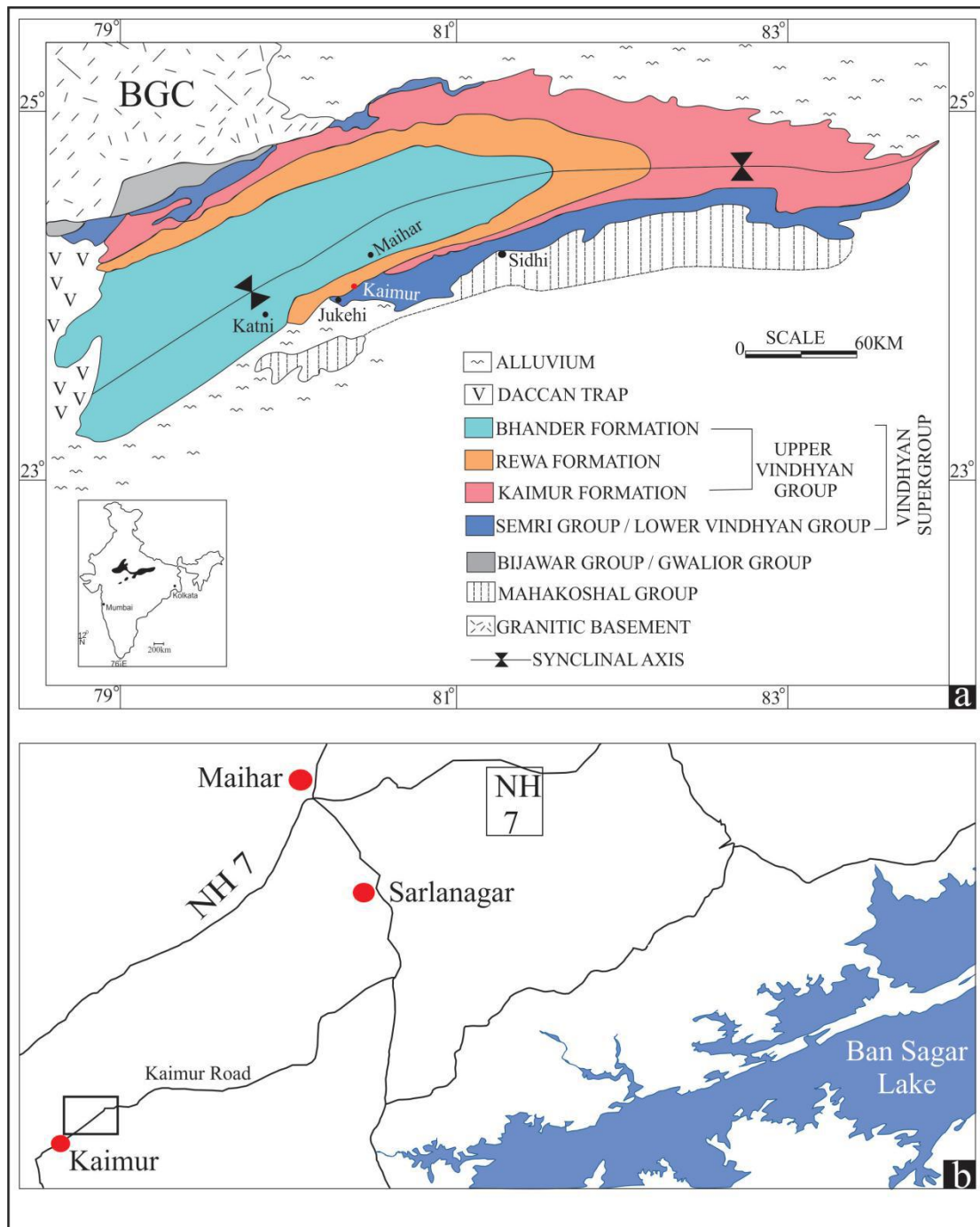


Fig 1.2. Geological map of son valley Vindhyan (modified after Auden, 1993) (a)
Location map of our study area (b) (marked by square)

1.2. Geological background:

1.2.1. General geology and structural disposition:

The Vindhyan Supergroup is the thickest Precambrian sedimentary succession of India and the duration of its deposition is one of the longest in the world. The Basin overlies the stable Bundelkhand craton of Archean-Early Proterozoic age (Tandon et al., 1991). The southern margin of Vindhyan basin is marked by a major ENE-WSW trending lineament termed Narmada-son lineament. Vindhyan Supergroup has been broadly divided into four Groups- Semri, Kaimur, Rewa and Bhandar, from the bottom to top. The Semri Group, also called Lower Vindhyan Group, is gently deformed and mildly metamorphosed and consists of carbonate-rich sediments. They are overlain by siliciclastics of later three Groups, i.e., the Upper Vindhyan Group. The Vindhyan are bordered by the Aravalli-Delhi orogenic belt (2500–900 Ma) (Roy, 1988) in the west and the Satpura orogenic belt (1600–850 Ma) (Verma, 1991) to the south and east (Fig. 1.3). The Bundelkhand massif (3.3–2.5 Ga) (Crawford and Compston, 1970; Mondal et al., 2002) occurs at the centre of the basin and divides it into two sub-basins-Son Valley in the east and Aravalli-Vindhyan in the west.

1.2.2. Tectonic framework:

Different ideas have been proposed about the tectonic setting for the Vindhyan sedimentation on the basis of piecemeal observations. Sedimentation in a foreland basin verging northward (Chakraborty & Bhattacharyya 1996) or southward (Chakraborti et al. 2007) was suggested. Some workers envisaged the Vindhyan Basin as a strike-slip fault basin (Crawford & Compston 1970; Crawford 1978). However, the general fine grain size, and high textural and mineralogical maturity of sandstones, defy rapid sedimentation from supracrustal source and do not comply with these suggestions. Extensive studies on multiple fronts later reveal intracratonic north–south rifting with a dextral shear at the initial stage (Bose et al. 1997, 2001) and sag at a subsequent stage (Sarkar et al. 2002). Consequently the east–west-elongated main Vindhyan Basin had initially been divided into several sub-basins by a number of NW–SE-oriented ridges (Bose et al. 1997), but during the Upper Vindhyan sag stage this segmentation was largely removed (Bose et al. 2001). A strong opinion exists that

the basin was east–west elongated, opening westward (Chanda & Bhattacharyya 1982; Sarkar et al. 2004).

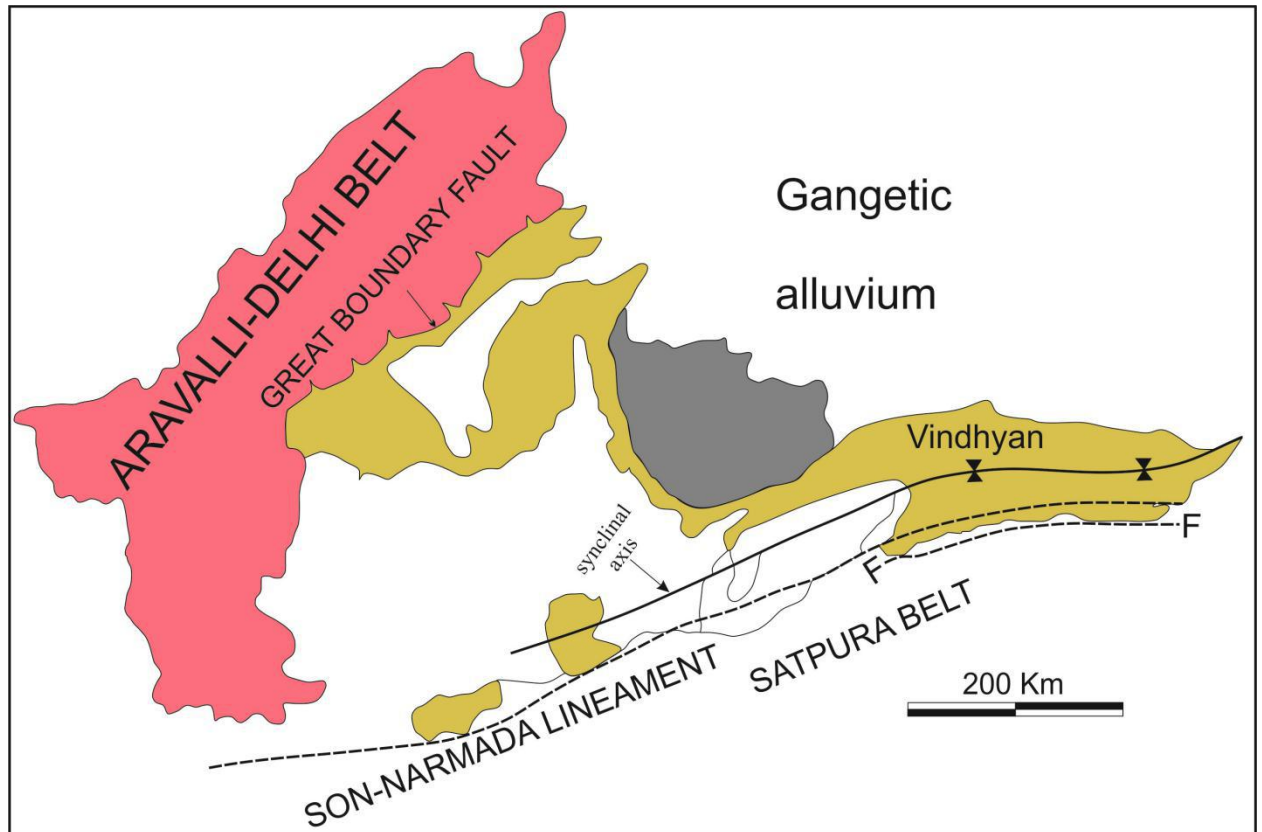


Fig 1.3. Tectonic framework of Vindhyan Basin

1.3. Stratigraphy:

The stratigraphic work of the Vindhyan Supergroup was started by Medlicott, 1859 and evolved through the works of Mallet, 1869, Oldham et al., 1910, Vredenburg, 1910 and Auden, 1933. The Vindhyan succession overlies the granitic basement/Mahakoshal groups of rock and underlies the Gondwana and Deccan trap and recent sediments. The entire Vindhyan succession, maximum thickness estimated to be around 3 km, and comprising mainly sandstone, shale and limestone is assigned as the Vindhyan Supergroup. The Vindhyan have been separated into 2 divisions which, though of very unequal proportions, have been determined by important physical considerations. They are separable as much by an unconformable junction between the two divisions as by the sharp lithological contrast between them. The lower division consists of one group and upper divisions have three groups. Thus the Supergroup is divisible into two groups on the basis of an unconformity:

1. Semri Group or Lower Vindhyan Group
2. Upper Vindhyan Group

Each group is again subdivided into several formations. The Semri Group in the Son valley rests unconformably on a variety of pre-Vindhyan rocks such as granites and metamorphics. In the Bundelkhand area, the group overlies the Bundelkhand Granite Gneisses and Bijawar Group of metamorphics, whereas in the southern Son valley, Mahakoshal is the basement in most places; however, in some localities (e.g., Deoland, M.P.) the basement is granite. The Semri succession of the Bundelkhand area has two detached outcrops around Chitrakut and Bijawar respectively, and is only a few tens of meters thick. The Vindhyan Supergroup is composed mostly of low dipping formations of sandstone, shale and carbonate, with a few conglomerate and volcanoclastic beds, separated by a major regional and several local unconformities. The regional unconformity occurs at the base of the Kaimur Formation and divides the sequence into two units: the Lower Vindhyan (Semri Group) and the Upper Vindhyan (Kaimur, Rewa and Bhander Formation). On the basis of lithological

distribution Lower Vindhyan/Semri Group and Upper Vindhyan have classified into several formations. Semri Group is divided into Deoland Fm., Kajrahat Fm., Porcellinite Fm., Khenjua Fm and Rohtas Fm. Kaimur Fm. Rewa Formation and Bhander Formation are within the Upper Vindhyan. Mathur (1981); Rao et al. (1981); Sastry and Mitra, (1984); Bhattacharyya, (1996) , Chaudhuri et al.(1998) said that the unconformity between the Upper and Lower Vindhyan is overlain by Bhagwar Shale, upper most unit of Rohtas stage/ Formation and underlined by Kaimur Formation .

It is generally believed that the Vindhyan basin was a vast intra-cratonic basin formed in response to intraplate stresses. The different depositional systems recognized in the Vindhyan succession are: alluvial fan, fan delta, braid delta, braidplain, eolian sand sheet, tidal flat (carbonate as well as siliciclastic), shoreface (tide and storm dominated), storm dominated shelf, homoclinal carbonate ramp, distally steepened carbonate ramp and epeiric peritidal flat (siliciclastic). The overall paleocurrent directions of the depositional systems in the Son valley are northerly suggesting a source towards south.

The unconformities divide the Vindhyan succession of Son valley into five sequences (Fig 1.1). Each sequence consists of several systems tracts representing different paleogeographic settings and marking paleogeographic shifts. The different strata of the Vindhyan succession show evidences of soft-sediment deformation suggesting syndimentary tectonic activity. The progressive and successive angular unconformities suggest that the deformation pattern shown by the Vindhyan strata is a reflection of syndimentary tectonic activity. It is postulated that the individual sequences of the Vindhyan succession are related to discrete episodes of tectonism that induced the subsidence necessary for accumulation of sediments and resulted into deformation of the older strata. Angular unconformities resulted due to erosion of the uplifted crest of the anticlines on which the next sequence of strata was deposited with an angular discordance.

There are sediment packages at the northern part of the Vindhyan basin developed from a northerly source and thus representing different tracts and sequences from

those of the southern part. These packages are represented intermittently in the succession and have been interpreted as representing periods of uplift of the Bundelkhand Granite and subsequent erosion in the north. The paleocurrents revealed by the Vindhyan strata are typically northerly suggesting that the evolving Satpura orogeny served as the source for the Vindhyan sediments. However, the source for the clastics occurring within the Semri Group and the lower parts of the Kaimur and Rewa Formation in the Bundelkhand sector was perhaps the Bundelkhand Granite Gneiss, Bijawar and Gwalior Group of rocks as manifested by the southerly paleocurrent direction.

Different authors have adopted different stratigraphic nomenclature for same litho units of Vindhyan Supergroup of rocks, which have generated a lot of confusions when considered in regional scale, and for correlation.

1.4. Stratigraphic problem in lower part of kaimur formation:

The entire Vindhyan sediments has divided into two parts eastern part i.e. Son valley Vindhyan and western part i.e. Rajasthan Vindhyan. The son valley Vindhyan has further subdivided into two sector Bundelkhand sector and Son valley sector (Chakraborty 2006; Chakraborty et al. 2010). An unconformity divides the Supergroup into two parts, herein referred to as the lower Vindhyan/Semri group and upper Vindhyan (Chanda and Bhattacharyya, 1982). However the exact stratigraphic position of the unconformity is still controversial. A number of workers previously noted that in Son valley sector, the top part of Rohtas Limestone gradually passes upward into Bhagwara shale which is composed of sand-silt alterations with substantial amount of pyroclastic sediments input (Chakraborty, 2006). Unconformity between upper vindhyan and lower vindhyan lies above this shale. Claim has also been made that the Sassaram sandstone observed above the unconformity in the Bundelkhand sector is absent in Son valley sector (Chakraborty 2006). During the present study of Kaimur, it has been observed that the position of unconformable contact is not same as previous observation. The study reveals the presence of sandstone having thickness approximately 12 m immediately above the Rohtas Limestone with a sharp, undulating and erosional contact in between. The sudden

change in depositional condition from that of a carbonate depositing environment to a siliciclastic one indicates a break in deposition. The unconformity should lie between Rhotas limestone and Sasaram Sandstone (Lower quartzite). So far the sandstone had not been described and detail sedimentological study of this sandstone is non-existent. Possibly this is the reason why most of the previous workers considered the Bhagwar shale within the lower Vindhyan group and placed the unconformity above it (Banerjee 1974; Sastry and Moitry 1984; Bhattacharya 1996; Chakraborty 2006; Valdiya 2010; Kumar and Sharma 2011).

1.5. Chronostratigraphy:

The Vindhyan Supergroup is the thickest Pre- cambrian sedimentary succession of India and the duration of its deposition is one of the longest in the world. The age of the Vindhyan Supergroup has been a matter of debate for over last hundred years. Venkatachala et al (1996) published a comprehensive review of geochronological information on the Vindhyan. In spite of minor inconsistencies the available data supported the conventional belief that the Vindhyan strata were deposited between the earliest Mesoproterozoic and latest Neoproterozoic (1400–600 Ma). Barring some indirect information from carbonaceous mega fossils and stromatolites (e.g., Kumar and Srivastava 1997; Rai et al 1997), most of the pre 1998 chronological information came from a large number of K–Ar ages, mostly from the work of Vinogradov et al (1964). Seilacher et. al. (1998) reported the oldest trace fossils of multicellular animal (non Ediacaran) in Chorhat Sandstone (Semri Group), which was believed to be 1100 Ma old based on K- Ar dating (Fig. 1.4). Recently quite a good number of radiometric age have been put forward for the Age of Vindhyan Supergroup.

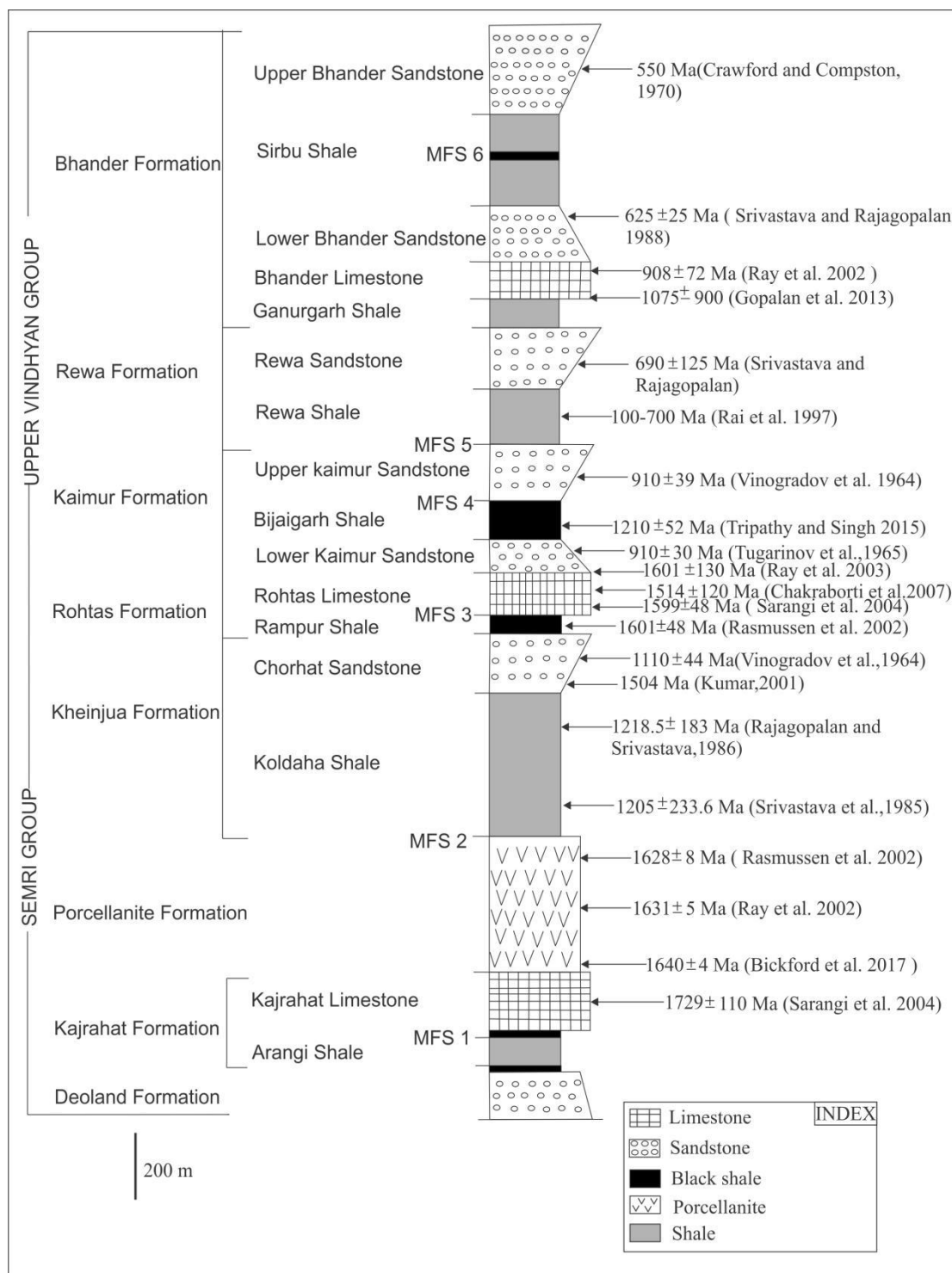


Fig 1.4. General lithology , age and stratigraphy of Vindhyan Supergroup (after Bose et al., 2001)

1.6. Lithostratigraphy, palaeogeography and sequence stratigraphy:

The Vindhyan sedimentary rocks are generally interpreted as predominantly shallow marine in origin. Dominant lithologies of this Supergroup are sandstone, shale and carbonate. Conglomerate is rare and almost exclusively intraformational. Major felsic pyroclastic deposits are present in the lower part of the Stratigraphy. The depositional palaeoslope was presumably gentle throughout the basin history. Palaeocurrent direction was consistently northward and indicates terrigenous supply from relatively low relief southern source. Palaeoclimate was probably warm and humid to facilitate elimination of the labile minerals.

There have been several attempts to visualize the depositional environments and the palaeogeographic set ups of Vindhyan Basin. Vindhyan Supergroup is dominated by near shore marginal marine, such as barrier bar, lagoon, tidal flat & beach deposits within intermittent subaerial exposure (Banerjee, 1964; Singh, 1976, 1985; Rao and Neelakantam, 1978; Chanda and Bhattacharya, 1982; Prakash and Dalela, 1982; Soni et al., 1987; Prasad and Verma, 1991; Akhtar, 1996, Bose et al., 1999, 2001, Sarkar et al., 2002 a,b, 2004). Banerjee (1974) invoked a “paired barrier island sedimentation” model for the Vindhyan in Son valley. He interpreted linear sandstone ridges comprising crossbedded mature quartzarenite as the product of barrier beach-dune complex, and limestone shales as lagoonal-tidal flat deposits on the landward side of the barrier island. Singh (1980, 1985) interpreted all the major Vindhyan sandstone units as shallow marine shoal complexes and fine grained clastics and carbonates as lagoonal tidal-flat deposits. Chanda and Bhattacharya (1982) argued that the whole Vindhyan was deposited in shallow marine environment, atleast within wind fetch. However shallow marine depositional framework appears to be very inadequately reconciled in terms of the mechanisms of crustal subsidence, basin development and sea level fluctuation. Bose and Chakrabarty (1994) identified fluvial and aeolian deposits in the Rewa formation delineating products of different flow stages and different sub-environments Aeolian longitudinal dunes, draas-interdraas complex, translent strata can be recognized in the upper part of the Upper Bhandar Sandstone in Rampur hill near Maihar (Bose et al., 1999). Process related study in marine segments

were conducted by Bose and Chaudhury (1990); Chakrabarty and Bose (1990, 1992a, b); Chakrabarty (1995); Chakrabarty (1995); Sarkar et al.(1996,2002a,b) and Bose et al.(1997 a) and shelf deposits have been documented at many stratigraphic levels. The only disconcerting view was that of Bhattacharya (1996b)who suggested that Vindhyan sedimentation took place entirely in terrestrial environment such as lacustrine, fluvial, aeolian, and refused his earlier emphasis on marine sedimentation. This view however did not receive favour from later workers. Only the rare patches of diamictite at the very base of the Supergroup have been attributed to glaciation by some workers (Dubey and Chowdhury, 1952; Chaudhury,1953;Ahmad,1955, 1958). Besides some reddish mudstone sequences at the top of the Supergroup bear Pseudomorphs of gypsum, anhydrite and salt indicating arid climate last lap of Vindhyan sedimentation.

Lower Vindhyan/Semri group has been persistently interpreted as the product of sedimentation in shallow marine and coastal environments (Singh,1973; Banerjee,1974). However, Chakrabarty et al.(1996), argued that the sequence was laid down in deep marine setting below the storm wave base. But Bose et al. (2001) conclusively proved it to be dominantly shelf deposit. Local patches of diamictite at the base of Deoland formation although has been attributed to glaciation, such hypothesis is questionable (Ahmad, 1958; Chaudhury, 1953; Dubey and Chaudhury, 1952; Mathur, 1954, 1960, 1981, 1989). There is no record of worldwide glaciation at that time. Chakrabarty and Bhattacharya (1996) have suggested that the conglomerates are mass flow products in a high gradient alluvial fan. The Deoland sandstone inferred as shelf sediment, fines upward and grades into the Arangi shale as of marine offshore origin (Bose et. al.,2001). Kajrahat limestone with profuse development of stromatolites was considered by Singh (1973) and Banerjee (1974) as tidal flat deposits, whereas Banerjee et al. (2007) described as it a shallow marine product. Volcanic tuff, pyroclastics surge and flow deposits make the Porcellanite formation and imply intrabasinal volcanism. Srivastva (1997) recorded sub-aerial volcanism whereas Banerjee (1997) recorded frequent sub aerial to sub aqueous transitions in the Porcellanite Formation. The Kheinjua Formation was entirely considered as lagoon-tidal flat deposition by Banerjee (1974) and Singh (1973). Sarkar et al. (1996 a,b) and Bose et al. (1997, 2001) recently indicated deposition in the shore face, fluvial and coastal aeolian environments. A tidal flat environment of

deposition was suggested for the Rohtas formation. Chakrabarty et al.(1996) considered Rohtas limestone even as a slope deposit from the preserved conglomerate horizons. On the contrary Chatterjee and Sen (1988) and Banerjee (1997) regarded the succession as open shelf originated. however Bose et al., 2001 recorded the presence of wave ripple sand shelf storm bed sand lateral pinchout of those conglomerate horizons and established shoaly upward trend in the Rohtas limestone.

The Upper Vindhyan in contrast to the lower Vindhyan is well studied. The Lower part of Kaimur Formation is shaley and lenticular in geometry. The basal sandstone incorporates tidal bars (Chakrabarty and Bose, 1990) and this interval passes up into a fining upward interbedded shale-sandstone succession ascribed to predominant storm deposition. The sand free organic rich and pyritic Bijaygarh Shale on the top of lower member is inferred as a deep offshore product (Chakraborty, 1993b). The entirely sandy upper Kaimur is now thought to be product of inner shelf to fluvial transition (Chakraborty, 1993a).

The Rewa Shale comprising the lower part of the formation is again a storm dominated shelf product (Chakrabarty et al., 1996, Chakraborty and Sarkar, 2005) resting on a thin granular lag blanket on top of the underlying Kaimur Formation. The upward transition from Kaimur formation to Rewa Sandstone infers shallow marine-tidal to fluvial/aeolian deposits (Bose and Chakraborty 1994). The younger Bhander formation is the only Upper Vindhyan deposit that has a laterally persistent carbonate deposit of thickness more than 80 m known as the Bhander limestone (Sarkar et al. 1996a). It is bounded below and above by Ganurgarh Shale and Lower Bhander Sandstone, interbedded mudstone-sandstone sequence. Both these bounding formations are reddish in colour, bear emergence features and salt crystals pseudomorphs, and are of probable coastal origin (Bose and Chaudhury, 1990; Chakrabarty et al., 1998). Between them the micritic, stromatolitic, intraclastic and Oolitic Bhander limestone is of shallow shelf product (sarkaretal.,1996, 1998). The Sirbu Shale overlies the Lower Bhander Sandstone gradationally and its basal part, comprising stromatolitic and oolitic patches enclosed by grey shale and showing emergence features, is interpreted as lagoonal (Singh,1973). This lagoonal shale is overlain by dark-coloured sand free shale showing no emergence features and is designated of shelf origin (Sarkar et al., 2002). Eventually the Sirbu Shale shelf

succession grades upward into the Upper Bhandar Sandstone, the youngest member of the Vindhyan Supergroup. It is entirely terrestrial but there are thin coastal storm packages at certain levels (Bose et al., 1999; Sarkar et al., 2004). Depositional environment, Palaeogeography and the system tracts are given in after Bose et al. (2001) (Fig. 1.1)

1.7. Objectives of the present work:

The present work has been framed with the following specific objectives in order to fulfill the required task.

1. Detailed fieldwork of the studied areas and to delineate its lithological variation through facies analysis.
2. Reconstruction of processes regrading each and every facies encountered in the present endeavor constructing its paleogeography and paleo-environment.
3. Geochemical analysis of glauconites present on top part part of Lower quartzite.
4. Study of Paleo redox and environment significance of glaucony origin .
5. Detailed study of Sequence development of study area.

1.8. Methodology:

Extensive field work was the main stay of the present work. For field purpose toposheet no 63 D/15 and 63 D/16 of G.S.I., clinometer-compass, measuring tape, diagonal scale, camera, hand- lens, hammer, chisel, geological knief was used. For petrographic characterisation SM-pole-Leitz microscope was used. Fresh sample was collected. Well preserved glaucony samples were studied under microscope (Leica DM2700P microscope attached with DEF450 camera) on polished slaps. Glaucony

samples were under SEM and EPMA. Quantitative oxide weight percentage were measured by EPMA in IIT Bombay Methodologies for gaining specific insight will be detailed or referred to when adopted. Field data were analyzed (Nikon 600 POL, Leica DM LP with Leica DC 300 FX) that facilitated the work enormously.

SOFTWARES USED: CorelDRAWX5, Open Rose V0.01, Microsoft Office.

Chapter 2

Facies analysis and depositional environment

Eliciting the depositional modes of the ancient sedimentary rock is an essential pre-requisite for the study of sedimentary rock. To achieve the goal by which one can infer the environment of deposition is always helpful to a sedimentologist. A facies analysis with potential for working out the genetic differences between co-existing sedimentary body as adapted here, would thus be more beneficial (Miall, 1980; Hallam, 1981; Walker, 1984; Reading, 1986). The identification of various sedimentation processes from deposits, or sedimentary facies, is crucial to the recognition and paleo-geographic reconstruction of ancient sedimentary environments. Sedimentary facies are visually distinguishable descriptive varieties of sedimentary deposits, with different facies indicating different modes of sediment deposition. For this purpose, sedimentology combines knowledge derived from studies of modern environments and laboratory experiments, and uses this knowledge to understand the origin of sedimentary rocks. Stratigraphic analysis of facies succession gives insight into the depositional processes, paleo-environmental conditions and development history of sedimentary basins, and allows prediction of the geometry, lateral extent and spatial distribution of sedimentary rock bodies.

2.1. Facies distribution of thick sandstone unit above Rohtas Limestone:

The ca.12m thick sandstone succession overlying on Rohtas Limestone (top most part of lower Vindhyan Group) with a sharp, erosional boundary. The boundary between Sandstone and the underlying Rohtas Limestone is demarcated by a thin (ca. 10 cm) sheet like unit containing pebbles of chertified limestone (Fig. 2.1).Overall grain size of this sandstone varies from coarse to fine sand. Considering the primary sedimentary structures, sediment composition and bed geometry the sandstone can be subdivided into two facies associations - (a) Facies Association I and (b) Facies Association II. The constituting facies of Facies Association I is in general of fine to medium size sandstone and also rich in mud compared to that of Facies Association II. Following are the detailed description and interpretations for each Facies Association of the sandstone(Fig 2.1a).

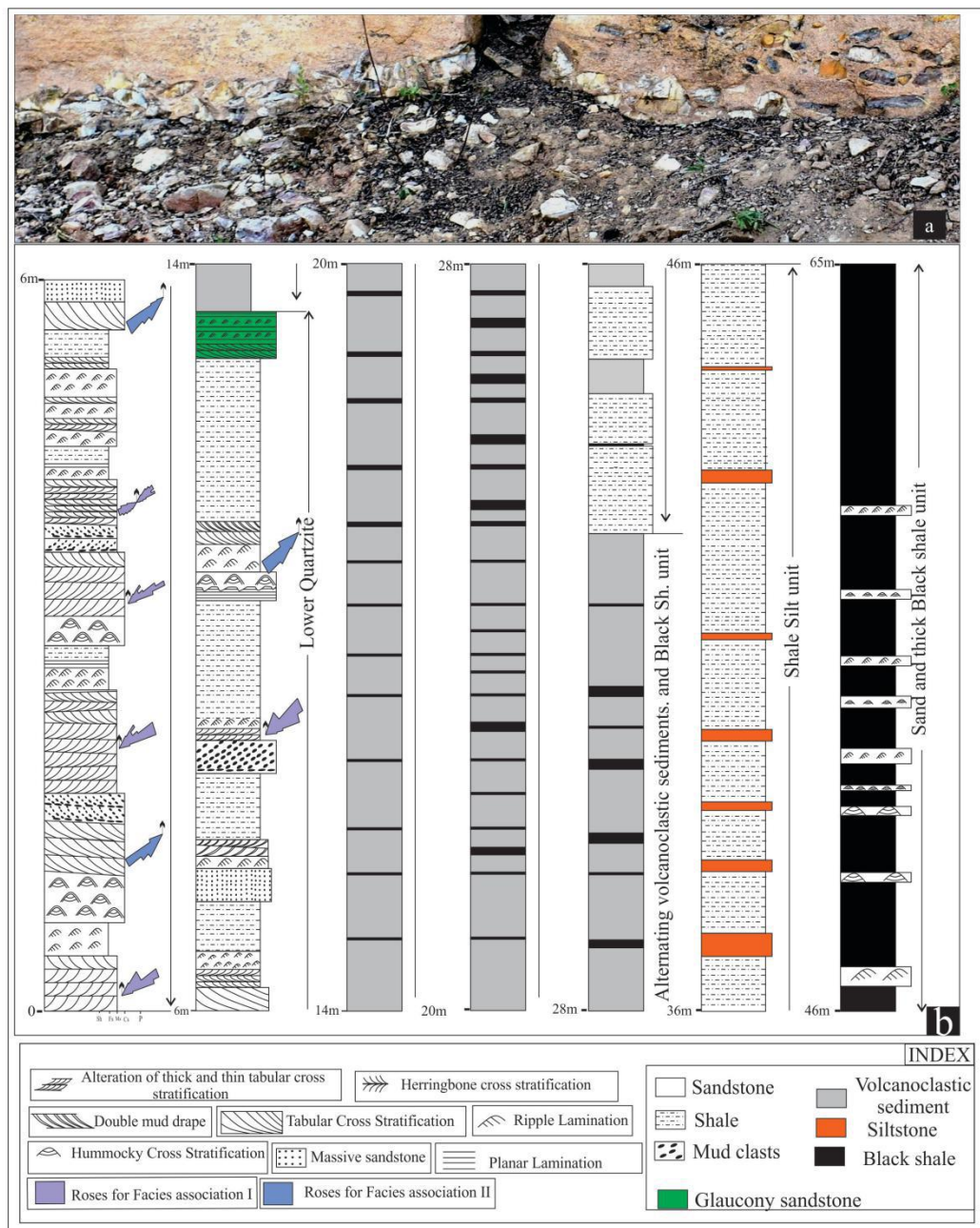


Fig. 2.1. Transgressive lag at the basal part of sandstone unit and above chertified Rohtas Limestone (a). Detailed log showing vertical facies distribution within the Loer part of Kaimur formation(b).

2.1.1 Facies Association I

Facies Association I is distinctly different from the facies association II with respect to grain size (varying from medium to fine sand) and mud content. This Facies Association I is dominantly cross-stratified and consists of following four facies-

2.1.1a. Alternation of thick and thin tabular cross-stratified sandstone facies:

This facies comprises medium to fine grained sandstone exhibiting unidirectional cross-stratification (Fig 2.2 a). It is present at the basal part of the sandstone and lies exactly on top of the basal thin and sheet-like pebble lag. Average thickness of the facies is 15 cm. Internally the cross-stratifications are characterized by alternation of thick and thin planar tabular cross-strata; the foreset bundles are separated by mudstone partings. The thickness of the individual foreset varies between 0.5cm and 3.2 cm whereas the mudstone laminae are sub-millimeter in thickness. Thickness measurement of cross-set bundles reveals a near symmetrical pattern of cyclicity. A maximum of 28 lamina occur between two successive peaks of the thick laminae (Fig.2.2b). Usually foreset dip decreases from the highest peak to trough of the sinuous curve. The dips of cross-sets decrease down current from ca. 30° to ca. 15° and laterally pass over into compound cross stratification at times (marked in Fig. 2.2c); Rouse, 1961; Bose et al., 1997). Some of the foresets are defined by mud clasts (Fig.2.2d). At places thick mud drapes (up to 2 cm) occur within cross-lamina set (Fig.2.2 g). Small-scale cross-lamina (ca 3 cm thick) dipping oppositely is occasionally present within the larger foreset of the cross-bedding.

2.1.1b. Herring-bone cross-stratified sandstone facies:

Two sets of oppositely dipping cross-strata separated by a gently inclined, planar erosional surface constituting a herring-bone pattern is another facies of this association. Average thickness of this facies is 30 cm. The orientation of herring-bone cross-strata shows distinct bi-polar and bi-modal palaeocurrent direction all over the studied stretch (Fig.2.2f). Double mud drape is a characteristic feature of the foresets. Mud clasts are present along the boundary between two differently oriented sets of cross-stratifications at places(Fig.2.2e).

2.1.1c. Small-scale ripple laminated sandstone facies:

This facies is characterized by small-scale ripple laminated sandstone and is commonly associated with the facies 2.1.1a. Mud is present at the trough of some of the ripples. The maximum thickness of the ripple foreset is 5cm. Thick mud partings occur at the ripple set boundaries. Ripple cross lamina exhibit sigmoidal pattern at places.

2.1.1d. Planar laminated sandstone facies:

Parallel laminated sandstone with intermittent mud laminae defines this facies. Average thickness of the facies is 20 cm. The facies exhibits vertical variations in lamina thickness (ca.2 cm for sand lamina and 0.3 cm for mud lamina). However, limited exposure does not permit measurement of thickness of sufficient numbers of laminae (Fig 2.2i).

Interpretation:

The presence of a thin lag between the Rohtas Limestone and the sandstone unit possibly represents a transgressive lag (Catuneanu, 2006; Mandal et al., 2014). Presence of the transgressive lag (Fig 2.1a) along the boundary of the Rohtas limestone and this sandstone indicate a fresh episode of sedimentation after the completion of lower Vindhyan sedimentation which ends with Rohtas Limestone. The internal structures of sandstone, cyclicity in laminae thickness and high concentration of mud within all the constituting facies of the facies association I indicates tide-dominated depositional setting. The bed load movement under the influence of dominant unidirectional current during the tidal regime is inferred. The alternations between thick-thin foreset superimposed on larger cycle strongly support tidal actions. Bipolar and bimodal paleocurrent direction of herring-bone cross-stratified sandstone facies corroborates tidal actions (Visser, 1980; De Boer et al., 1989, Bose et al., 1997). Presences of double mud drapes (Fig 2.2g) within this facies indicate a subtidal environment (Visser, 1980; Bose et al., 1997; Eriksson and Simpson, 2004, Kohseik and Terwindt, 1981). The larger cycle, measured from alternating thick-thin laminae, is very much compatible with the lunar bi-monthly (spring to spring) cycle (Fig2.2b).

This can readily be attributed to semidiurnal tides. The intra-set cyclic variations along with grain size indicate repeated waxing and waning of the water flow. In contrast to the bidirectional paleocurrent pattern, alternating thick-thin tabular cross-stratified sandstone facies is unidirectional in nature which indicates flow reversal possibly left imprint during abandoning phase of tidal sand-waves (Nio and Young, 1991; Bose et al., 1997). In places mud laminae within the constituting facies are very thick. Such thick mud drapes in between the sand layers are difficult to form at any stage of tidal cycle (McCave, 1985; Chakraborty and Bose, 1990). However, thick mud can be introduced to any tidal system from outside by a process which is able to disperse mud in suspension load from the shoreline environments, possibly by a super-storm event (Allen, 1988; Chakraborty and Bose, 1990). High suspended sediment concentration may lead to deposition of thick mud layer during neap period as well (Schieber, 1986).

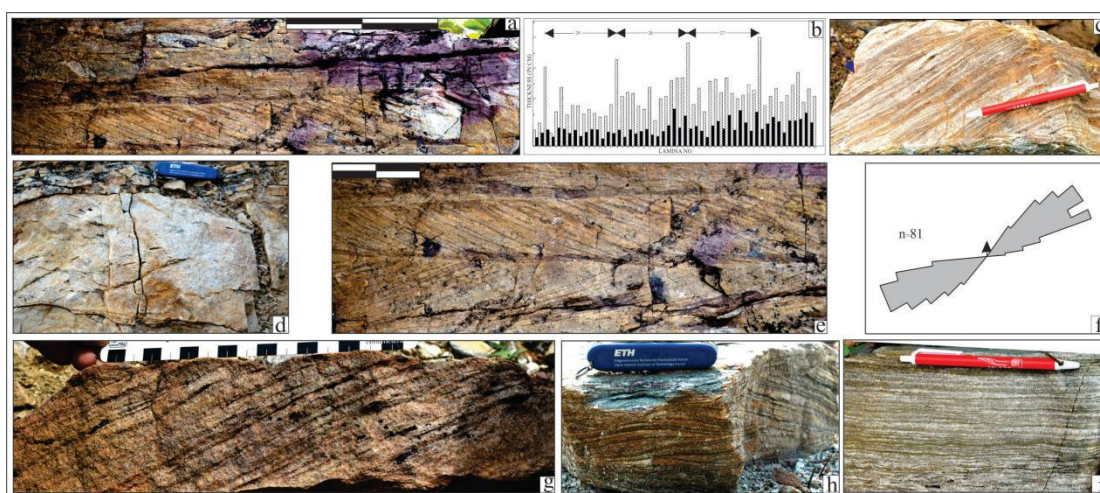


Fig.2.2. Photographs of facies association I in the sandstone unit above Rohtas limestone: Thick thin alternating tabular cross stratified sandstone (a) (bar length 20 cm). Cycle of thick-thin alternation (b). Composite cross stratification (c) (N.B. small scale cross stratification are dipping oppositely) (length of the pen 15 cm). Mud clast orientation along the cross stratification (d) (scale of the knife 8 cm). Herringbone cross stratification (e). Rose diagram of herringbone cross stratification (f). Double mud drape (g). High concentration of mud in the ripple trough (h). Planer laminated sandstone (i)

2.1.2. Facies association II

This association occasionally interferes with the Facies Association I. However, Facies Association II, characteristically contains less mud compared to Facies Association I. Facies Association II primarily consists of coarse to fine-grained sandstone. Five facies comprising of the Facies Association II are discussed as follows:

2.1.2a. Massive sandstone facies:

This facies is characterized by massive, coarse to medium grained sandstone beds (thickness of the facies is ~ 20cm) (Fig2.3a). The base of the facies is sharp than its top. Gutters, bipolar prod marks and locally flutes are present at the sole of this facies. The massive beds often grade upward into planar laminated beds followed by cross-stratifications. Overall grain size of the facies decreases upward. Mud clasts are common at the base of the massive beds as well as along the cross-stratifications. The style of cross-stratification within a set changes laterally but non-cyclically. The brink point of the cross-stratifications maintains nearly the same distance from the base. The top of the sandstone beds are invariably wave rippled. The ripple crests are straight in nature, having local bifurcations, although discernible asymmetry is common in their profiles.

2.1.2b. Tabular cross-stratified amalgamated sandstone facies:

This facies is characterized by amalgamated sandstone beds(Fig.2.3d). Maximum thickness of individual bed is ca. 32cm but amalgamation may contribute a thickness up to 1 m. Internally tabular cross stratifications define these amalgamated sand beds. Paleocurrent direction measured from these tabular cross-strata is directed towards WSW direction. It is commonly associated with massive to feebly graded sandstone facies and hummocky cross stratified sandstone facies. The bases of the facies are sharp while their tops are gradational with occasional presence of wave-ripple laminations.

2.1.2c Hummocky cross-stratified sandstone facies:

This facies is characteristically medium- to fine-grained, moderately sorted sandstone with broadly lenticular to tabular beds with convex-up tops (Fig.2.3e). It is overlain by wave ripple laminated facies with less sharp contact. Hummocks and swales are frequently observed with maximum height and wavelength ca.8 cm and 35 cm respectively. Bases of such beds generally replicate the underlying bed surface. Hence the bases are sharp but non-erosional whereas top of the beds are less sharp. This facies is commonly associated with the top part of the Massive sandstone facies. Overall normal gradation is observed within the facies.

2.1.2d Wave ripple laminated sandstone facies:

This wave ripple laminated sandstone facies generally overlies the top of the preceding facies. Ripple crests are straight and show bifurcations on the bedding plane. Syneresis cracks are abundantly present on the bed surfaces of these beds at different levels. Overall orientations of these cracks are fairly consistent but vary widely between beds (Pratt, 2002)

Interpretation:

Considering all the structures, stacking pattern of beds within the facies of this association, it can be inferred that tide dominated environment was occasionally interrupted by high energy events like storms. The massive sandstone facies indicates rapid dumping of the sediments. Massive character, absence of normal grading or post depositional liquefaction indicate that they must have been deposited by short-lived high density flows and because of the faster rate of sedimentation hydraulic sorting process failed to operate (Kneller and Branney, 1995; Magalhães et al., 2015).

Occurrence of amalgamated sandstone beds within Facies Association II, juxtaposed one above other suggests rapid occurrence of an event flow, possibly storm surges, in a high flow regime (Sarkar et al., 2004). The individual sandstone bed comprising amalgamated sandstone facies indicates product of a single depositional continuum over a relatively short time. Sharp irregular base with sole features also

supports the high energy events responsible for deposition of the beds and supercritical nature of the initial flow (Sarkar et al., 2012). The cross-stratification

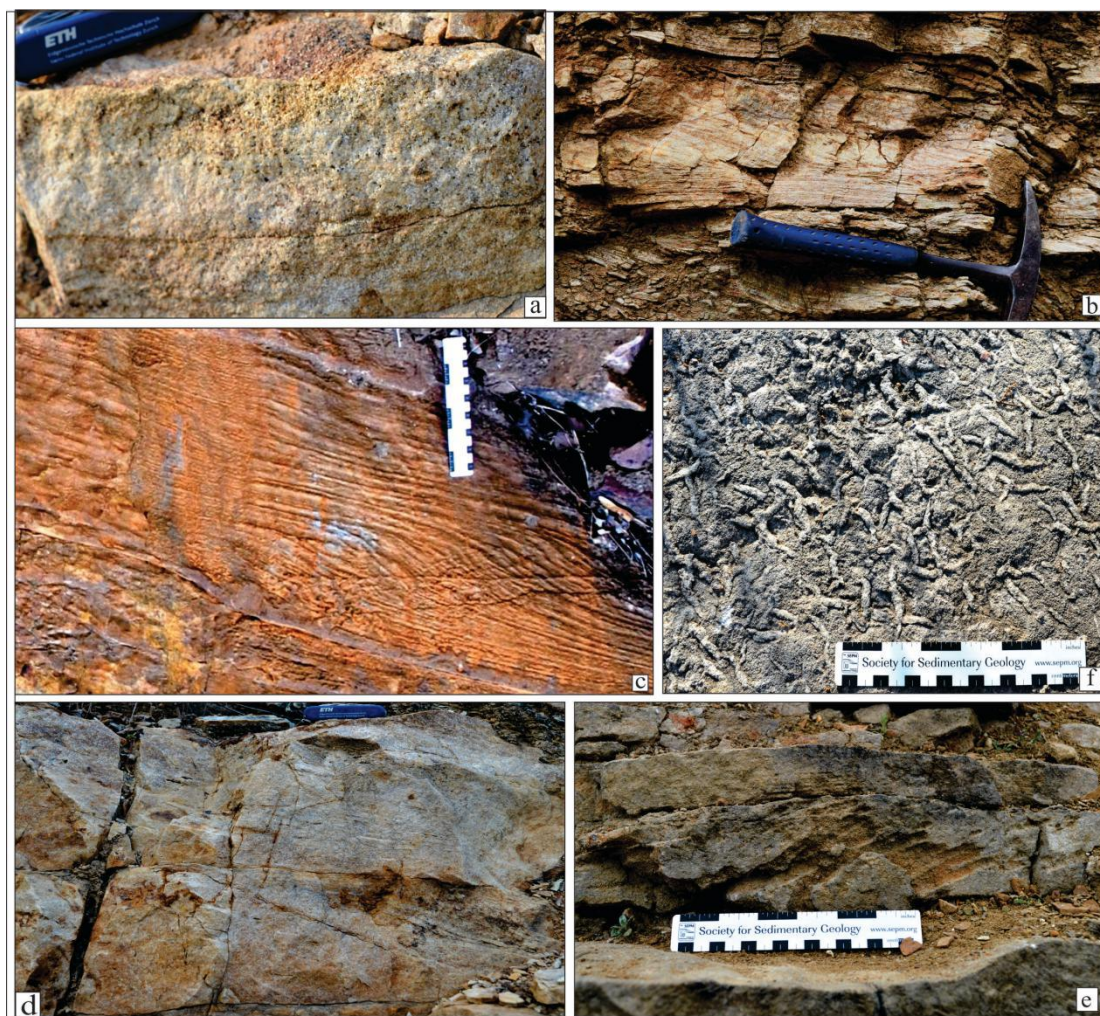


Fig. 2.3. Photograph of facies association II. Massive sandstone(a). Transition of planar laminated sandstone to cross stratified sand stone (b). Brink point of cross stratification maintaining same level on the base (c) Amalgamated cross stratified sandstone(d). Hummocky cross stratified sand stone (e). Syneresis crack on the bedding surface of sandstone (f)

having the brink points at same height from base (Fig. 2.3c) suggest high rate of sand fall-out from suspension possibly during the periods of heavy storm. The steady upward decline in both grain-size and flow regime suggests gradual waning of the high energy events (Bose and Sarkar, 1991). Preserved wave ripple forms on the bedding surface and hummocky cross-stratified sandstone facies clearly reflect deposition under the influence of oscillatory flow possibly during storm surges.

Asymmetry in the ripple profiles indicates simultaneous presence of a tractive force within the flow. Deposition from storm generated combined, wave-cum-current, flow is thus inferred. Syneresis cracks (Fig.2.3f), present on the bed-surfaces of wave ripple laminated sandstone facies possibly originate through dewatering of the sandy beds due to rapid deposition of the overlying sediment (Kidder, 1990). Increased pore-water pressure because of storm wave action (Cowan and James, 1992, Harazim et al., 2013, McMahon et al., 2017) may be responsible for the generation of syneresis cracks.

Discussion:

The Rohtas Limestone is the top most unit of Lower Vindhyan succession. The limestone is overlain by laterally persistent sandstone in the studied stretch of the Son valley. The sandstone deposited on an undulating surface over a transgressive lag formed on the top surface of Rohtas limestone. The majority of the clasts present within the lag derived from the Rohtas limestone. Majority of the lime-clasts are chertified. The topmost part of the Rohtas limestone is also chertified at places. The degree of chertification also varies laterally to a remarkable extent. The chertified layers thus often appear to have irregular geometry and boundaries difficult to trace. Often they appear laterally discontinuous. Only exposure or near-exposure on earth surface can account this much abundance of silica during post depositional alteration or weathering of the limestone. It is likely that part of the Rohtas limestone was exposed for a long period of time which helps chertification (Kolodny et al. 1980). However, the transgressive lag indicates a fresh initiation of a new sedimentation event. The sedimentation started on a tide dominated shelf. The presence of thick-thin alternation, double mud drape layers and herringbone cross stratification, reactivation surface and frequently present mud lamina within the cross-strata are the tell-tale evidences of tide domination in the encroaching sea. This tide dominated environment intervened by storm as evidenced by the presence of hummocky cross stratification, amalgamation of sandstone beds, conglomerates/ massive beds with sole features. The presence of numerous sand-clasts within the facies association II supports the influence of micro-biota to make non-cohesive sand into a cohesive one (Sarkar et al. 2014, 2018) and likely to be deposited in a shallow marine environment. Vertical transition of the facies assemblages rules out any major Paleogeography shift. Some

of them indicate clear evidence of subtidal deposition while a shallow marine depositional environment can be inferred from the sandstone in general.

2.2 Facies distribution of silt (fine) and shale (black) alternations:

This sedimentary unit is dominated by alternation of shale and silt deposition. Siltstones are very fine grained and characterized light color tabular beds with two sets of joints. In an alternation of siltstone both grey and black shale beds have observed. Grey shales are present in the lower part of this succession while the black shales dominant in the upper part of this succession. Thickness of this succession is ca. 35 m. Both the fine siltstone and black shale beds are tabular in geometry. Siltstones beds have appeared in variable thickness from 5 cm to 40 cm. Siltstone beds are gradationally passes into black shale whereas the contact between black shale to siltstone is very sharp. The following facies have identified from this succession. Altogether these facies have nomenclature as facies association III.

2.2.1. Facies association III:

2.2.1a. Planar laminated grey shale:

This facies is characterized by planar laminated light color shale. Thickness of this facies varies from 15 cm to 5 cm. Shale beds have tabular geometry. It is associated with planar laminated black shale and ripple laminated shale. Laminations thickness are 0.1 mm to 0.3 mm. Some millimeter scale ripple forms are also preserved in this facies.

2.2.1b. Planer laminated thick thin fine siltstone:

This facies is constituted by alternating thick and thin beds of fine siltstone (Fig. 2.4c). Thicknesses of the thick beds are varying from 50 cm to 20 cm and they are tabular in geometry. Thin beds are very finely laminated and thicknesses of each bed are ca. 0.2 cm. This facies is mainly associated with planar laminated black shale facies though association with grey shale is uncommon. These beds contain very sharp contact with its associated facies when it deposited above other facies. Under microscope some crinkle laminations and false cross bedding has been observed in these beds.

2.2.1c. Ripple laminated fine siltstone:

Ripple laminated facies is another major facies in this succession. This facies is mostly restricted to the lower part of this succession. It is associated with planar laminated grey shale and planar laminated thick thin fine siltstone. Maximum thickness of this facies 25 cm. Planar laminated fine siltstone beds contain very sharp contact with planar laminated facies and gradation relationship with planar laminated thick thin fine siltstone beds. Very small scale cross stratifications are present in transverse section of these facies.

2.2.1d. Planar laminated black shale:

Black color, fine grained shale dominantly present in this facies (Fig.2.4d). Planar laminations are very prominent in this facies. This facies is also associated with planar laminated thick thin fine siltstone facies. Thickness of this facies is ca. 10 cm. High abundance of microbial growth has observed in this facies. Microbial laminae are either convergent or divergent and contain huge pyrite grains. Some time they are crinkly laminated.

Interpretation:

Abundance of shale in this facies association infers deposition was took places in a low energy environment. Shale has deposited in lowest energy regime, mostly deposited from suspension mode. Alternation of fine silt with shale indicates energy condition of depositional site fluctuated with time. Planar laminated fine siltstone in thick thin alternation with sharp contact indicates a sudden change of energy condition. But absence of any scour, sole mark, tool marks in these fine siltstone beds indicates energy condition was not high enough to form the negative structures. Ripple laminated siltstone indicates wave dominance. Abundance of black shale with fine siltstone indicates depositional site clam, quite and anoxic. Crinkly laminations infer deposition must have taken place within photic zone. Presence of pyrite with black shale is an indication of anoxic condition. So, we can infer that deposition was took place in a marine condition. Presence sand free shale infer deposition was took place quite deeper portion of marine, at least below the storm wave base. Black shale infers marine was that much deep where anoxic condition can prevail.

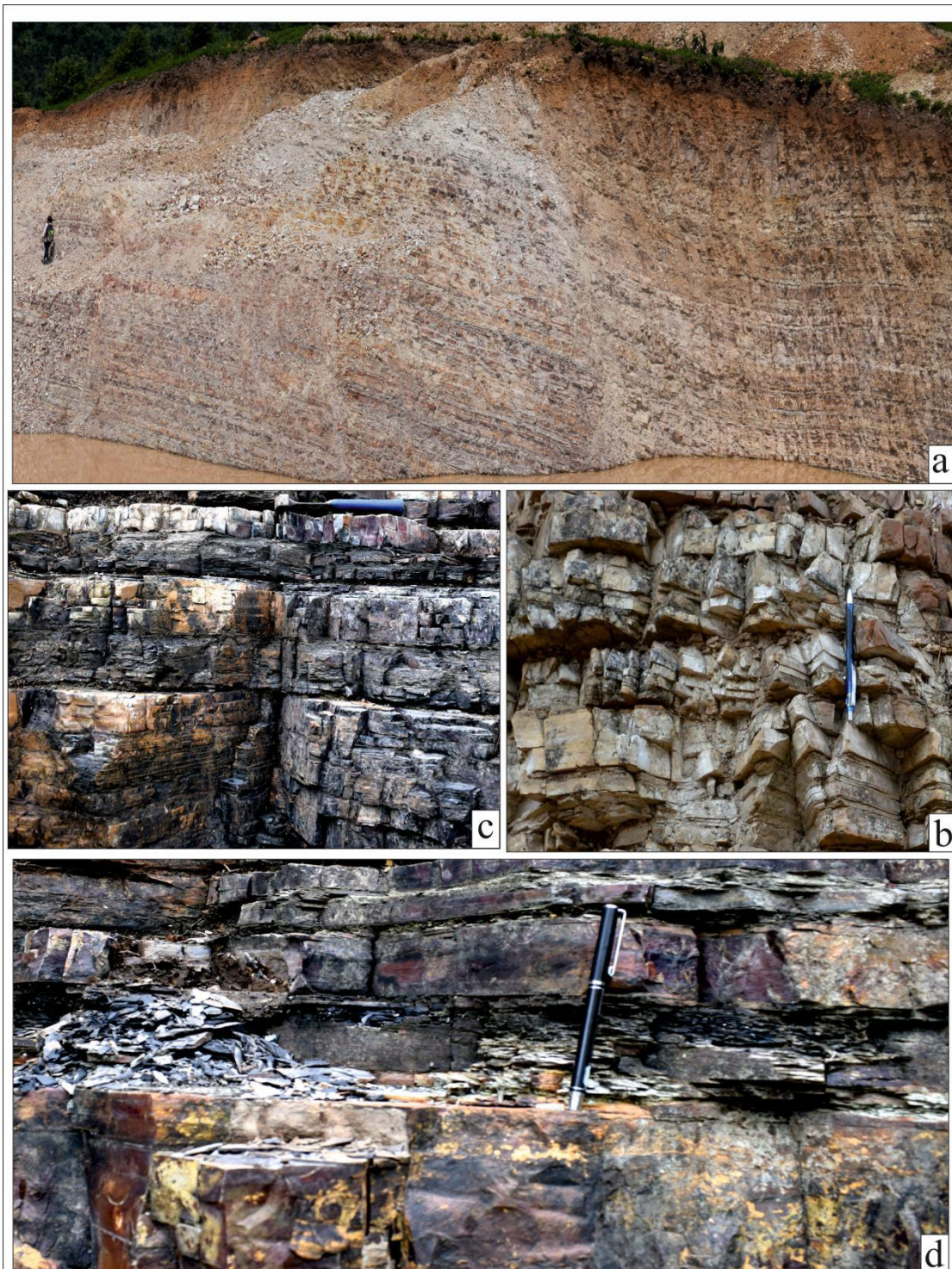


Fig. 2.4. Photographs of facies association III. Panaromic view of alternating fine silt and black shale unit (a). Two sets of joints in tabular silt stone beds (b). Planer laminated thick-thin fine silt stone (c). Ripple laminated silt stone with planer laminated black shale (d)

2.3. Facies distribution of “siltstone succession” above alternating “fine silt and black shale deposit”:

This sediment succession overlies on the alternating black shale and fine siltstone unit with a gradational contact. This unit is also persistent with tabular geometry. Initial sedimentation of this succession is grey shale. The grey shale gradually transits to pure siltstone. The vertical succession shows decreasing shale: siltstone i.e. from 8:2 to 4:6. Average thickness of this succession is ca. 10 m. Depending upon the primary sedimentary structures along with grain size variability the following facies has been classified.

2.3.1. Grey shale:

Grey shale with planar lamination is the most dominating facies distribution of lower part of this unit. Shales are very finely laminated. Average thicknesses of these beds are 30 cm. Few siltstone beds are associated with facies with very sharp contact.

2.3.2. Planar laminated siltstone:

This facies is also abundant in the lower part of this depositional unit. It is characterised by planar laminated fine grain siltstone (Fig 2.5b). Siltstone beds are tabular in geometry with a sharp contact of lower shale facies. Average thickness of these beds is 3 cm.

2.3.3. Ripple laminated siltstone:

Ripple lamination facies is mainly characterised by silt size grain and consists of ripple laminations. Thickness of these beds is ca. 4 cm. Ripples are sinuous in nature. Bifurcations of crests are observed on the bedding surface. A sharp contact is observed at the lower boundary between shale and siltstone beds. The abundance of this facies has increased upwards.

2.3.4. Cross laminated siltstone:

This facies has concentrated on the top part of this deposition. Cross stratifications

(Fig. 2.5c) are tabular in nature. They are associated with ripple laminated siltstone and grey shale. Contact between grey shale is very sharp, erosional. A gradational contact is observed with ripple laminated siltstone.

Interpretation:

All the sedimentary features and grain size distribution of studied unit indicate deposition was took place in a marine setting. Abundance of both shale and silt bed infer depositional site has energy fluctuation. Deposition of shale infers low energy, suspension fall out deposit. Presence of ripple lamination in the association of shale with sharp contact conveys a sudden energy fluctuation. Sinuous nature and bifurcation of ripple crest infer deposition was took place in wave dominated condition. The tabular cross stratified siltstone beds was deposited in the influence of tractive current. Presence of sharp, erosional contact at the lower part of the cross stratified siltstone indicate deposition was took place in a high energy condition. This high energy condition may be storm surge. The presence of ripple lamination above cross stratified beds signifies waning nature of the flow.

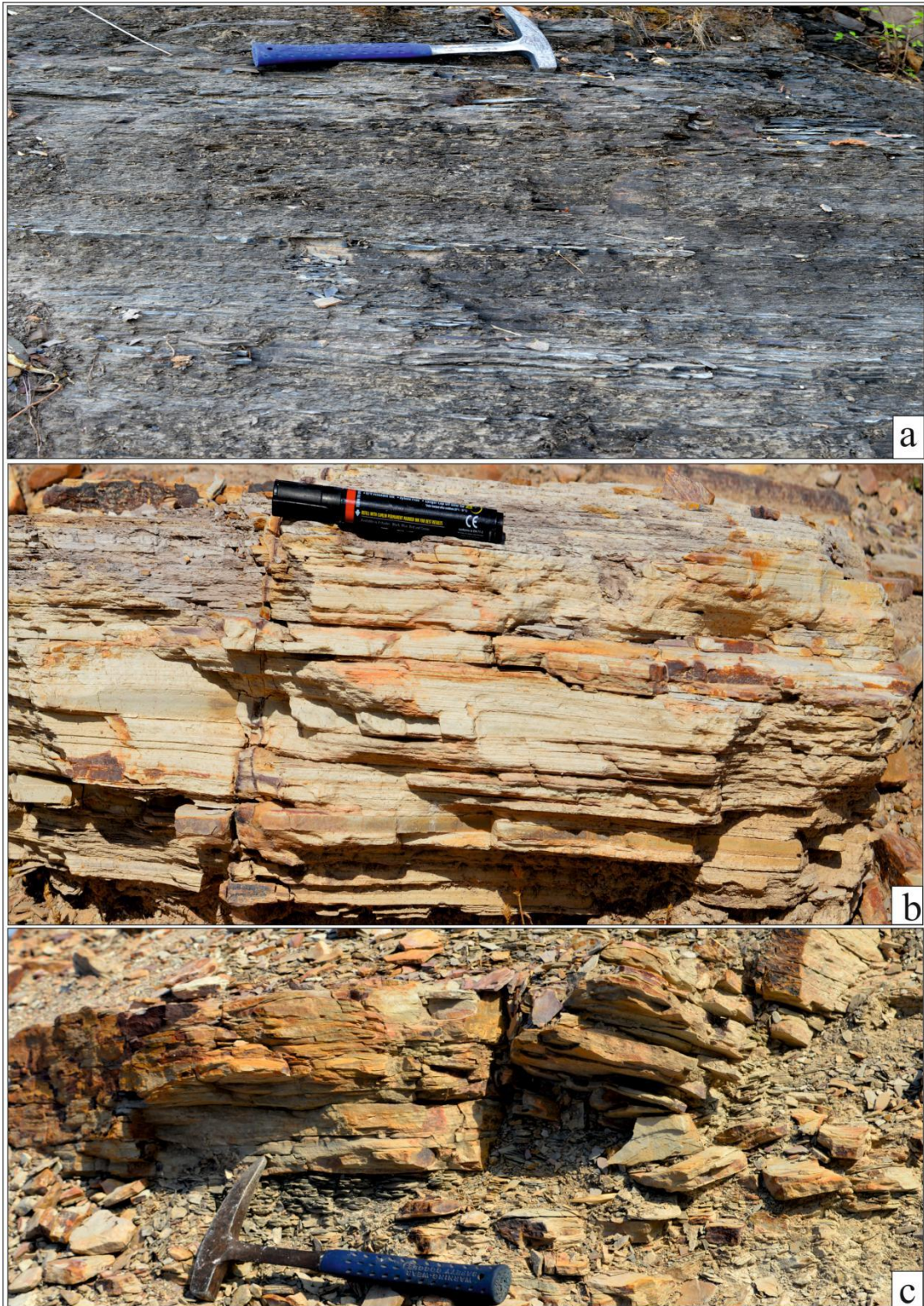


Fig. 2.5. Photographs of siltstone unit. Thick grey shale (a). Planer laminated silt stone (b) Cross stratified silt stone (c)

2.4. Facies distribution of thick grey to black shale deposit:

This sediment unit is characterized by numerous alternations of black shale and fine sandstone. The shale: sandstone ratio increases upward in the section gradually (Fig. 2.6c).

2.4.1. Planar laminated black shale:

This facies characterised by black, sulfidic shale, is absolutely free of sand and silt (Fig 2.6a). In outcrop sections the Black shale shows laterally persistent and uniform 3-5 cm thick bands. The bands are sharp based and internally characterised by upward gradational transition from a massive to weakly fissile part. The concentration of sulfur is higher in the fissile part than in massive part.

2.4.2. Hummocky cross stratified sandstone:

This facies is at the base of black shale and is represented by the large-scale hummocky cross stratification (wave length-0.3-5 m, amplitude 4-30 cm) along with its small scale variety (wave length 20 cm, amplitude 2 cm). The grain size of these sandstones ranges from 0.15 to 0.04 mm. The HCS may be symmetric or asymmetric in profile.

2.4.3. Gutter casts bearing sandstone:

The facies is characterised by numerous alterations between black shale and fine sandstone. The sandstone beds are sharp based contain abundant sole marks (Fig 2.6b) such as grooves, flute, gutters, prod marks, bounce marks. The scour is mostly elongated. In transverse section the inclination of wall of gutters varying between 10^0 - 70^0 ; their width and depth range between 2-6 cm and 2-40 cm respectively. The grooves are also long linear features, with their depth and width ranging from few cm to few mm. The prod marks are small scale, strongly asymmetric, and they occur on the floors of large scale scours. The scours are mostly filled with fine to medium grained laminated sand.

Interpretation:

The depositional features of sandstone indicate that they were deposited from episodic storm surges in a mud depositing environment, the intervening black shale being the products below the storm wave base. Anisotropic HCS along with low angle cross strata suggests operation of unidirectional currents along with oscillatory motion. The features of black shale represent deposition in the distal outer shelf environment where sand and silt could not be delivered even during storms. Anoxic condition is indicated by high content of organic carbon and the occurrence of syngenetic pyrite within the black shale. The massive parts are products of rapid deposition from muddy suspensions driven by storm flows, while the fissile parts are products of slow settling of mud in normal condition. The depth of deposition of black shale can logically be estimated to be greater than 80 m, perhaps around 100m.



Fig. 2.6 Photographs of Black Shale unit. Thick Black shale (a). Flute cast (b)

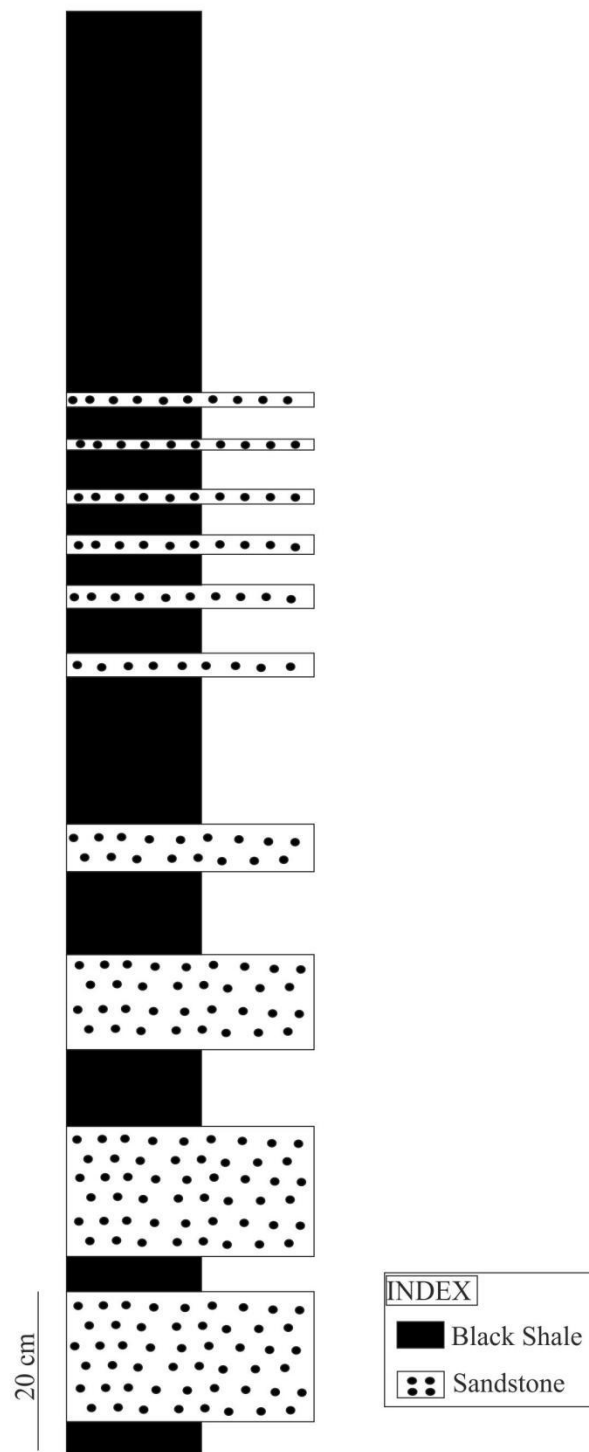


Fig. 2.7. Black shale increases upward gradually

Chapter 3

Geochemical analysis of Glaucony on top most horizon of Lower quartzite

Fe-Mg bearing dioctahedral glaucony minerals form in the active exchange of cations in sea-water and pore-water in a marine condition though formation of glaucony in other environment is not uncommon. Along with the authigenic glaucony allocthenic glaucony is also useful to study as the glaucony don't change its chemical composition once it stabilizes. The glaucony has changes its chemical compositions through time as the chemical composition has changed. The chemical composition of authigenic glaucony of same period may differ with one another being variable chemical composition of sea-water, change of sediment substrate. Differential co-ordination number and charge distribution of cations divide the cations into interlayer cations, octahedral cations and tetrahedral cations. In all of these cations K and Fe are the most important as their modal percentages are directly linked with evolution path of glaucony, sediment substrate and depositional environment (Amorosi, 2013, Banerjee et al., 2015, 2016a, Bansal, 2017). Simultaneous appearance of Fe^{2+} and Fe^{3+} in octahedral sites gives the opportunity to study the paleo-redox condition during glauconitization. The study of paleo-redox during glauconitization and its co-relation with depth range is very critical as the modern marine glaucony deposits in the depth range of 50-500m but mainly restricted within 200-500m (Odin and Matter, 1981) i.e. below photic zone though there are report of shallow water glaucony in ancient time (Banerjee et al., 2008; Tang et al., 2017). Amorosi (2013) claimed the authigenic glaucony are mainly restricted in 'ommission surface', 'condense surface' and 'mega condense surface' and the surfaces are co-relatable with sequence stratigraphic surfaces.

Present study investigates the genesis of glaucony in Mesoproterozoic Lower quartzite siliclastic deposition, depth range of glaucony deposit and paleo-redox condition of Mesoproterozoic Lower quartzite depositional ocean. Authors correlate this glaucony horizon with sequence stratigraphic surface. Mesoproterozoic Lower quartzite glaucony has compared with other Precambrian glauconite and puzzle out the low concentration of TFe_2O_3 and high concentration of K_2O and Al_2O_3 .

3.1. Materials and method:

The glaucony samples were collected from the lower most member of Kaimur Formation. Well preserved glaucony samples were studied under microscope (Leica DM2700P microscope attached with DEF450 camera) on polished slaps. Samples were under SEM and EPMA. Quantitative oxide weight percentage were measured by EPMA in IIT Bombay. $\text{Fe}^{2+}/\text{Fe}^{3+}$ ratio of glaucony were measured by titration process (Kelly and Webb, 1999). Glaucony minerals were separated from samples using magnetic separator and stereo microscope.

3.2. Mode of occurrence:

Lower quartzite glaucony, concentrate on the top most sediment deposit of Lower quartzite is ca. 70 cm thick. In field observation green sands appears along planar laminations and cross stratifications (Fig. 3.1a, 3.1b, 3.1c, 3.1d). In the closer look under microscope glaucony also maintains the laminations (Fig. 3.1e). Glaucony materializes in two different forms like boundaries of feldspars and linear stringers of feldspar's fracture and cleavage (Fig. 3.1e, 3.1f, 3.1g, 3.1h, 3.1i). In most of places, glauconitization fully replaces feldspar grains (Fig. 4f). In few places glaucony surrounds feldspar grains (Fig. 3.1g, 3.1h, 3.1i). The glaucony are interconnected with each other, 200 mm long and 0.2 mm wide. Glaucony are light green color under plane polarized light and third order light green to dark green under cross polarized light.

3.3. Major element composition and structural formula of glaucony:

Major elements oxide composition has determined by EPMA analysis in 75 points. Calculating the structural formula of glaucony, the $\text{Fe}^{+2}/\text{Fe}^{+3}$ ratios has measured 0.8 (measured by titration technique). Determination of elements were calculated on an anion equivalent basis to the structural formulae per $\text{O}_{10}(\text{OH})_2$. All analysis has been normalized to 100% on an anhydrous basis for different cross plot. The K_2O content in studied glaucony is restricted within a narrow zone, varies from 6.69 wt% to 8.27 wt% (Table 1). The high K_2O content in glaucony minerals recommended as "evolved" to "highly evolved" (Amorosi, 1997, Odin and Matter, 1981, Amorosi,

2012). Also “evolved” to “high evolved” glauconite suggest they are in mature stage (Amorosi et al., 2007, Amorosi, 2012). The low TFe_2O_3 content in glaucony minerals varies from 4.50 to 9.60 wt%. The low TFe_2O_3 in Lower quartzite glaucony is not co-relatable with evolved glaucony i.e. higher proportion of K_2O . Low TFe_2O_3 with high K_2O in Lower quartzite glaucony is similar to other Precambrian glaucony succession (Dasgupta et al., 1990, Deb and Fukuoka, 1998, Guimaraes et al., 2000, Ivanovskaya et al., 2006, Banerjee et al., 2008, 2015, Zhou et al., 2009, Drits et al., 2010, Sarkar et al., 2014, Tang et al., 2017). Lower quartzite glaucony contains high K, high Al, high Mg and low Fe. The cross plot of K_2O vs TFe_2O_3 falls within the ‘illite minerals’ (Fig. 3.2a) though some are within the field of “compositional gap” in Odin and Matter (1982) classification of glaucony minerals.

The cross plot of Al versus TFe ($r^2=0.69$) and Al⁺³ in octahedral versus Fe⁺³ ($r^2=0.64$) show negative relations (Fig. 3.2b, 3.2c). These negative correlations indicate substitution of Al⁺³ cations by Fe⁺³ cations in octahedral sites (Odin and Matter, 1981, Velde, 1985, Bornhold and Giresse, 1985, Dasgupta et al., 1990, Amorosi et al., 2007, Banerjee et al., 2008, 2012a, 2012b, 2015, 2016b, Chang et al., 2008, Tang et al., 2017, Bansal et al., 2017, 2018, Rudin et al., 2019). High MgO content (2.18 to 3.85wt%) in Lower quartzite glaucony is similar to other sediment succession in Vindhyan basin (Banerjee et al., 2008, Sarkar et al., 2014) and other Precambrian deposits (Tang et al., 2017) as well. The cross plot of Mg versus K has no such correlation. High Mg of Lower quartzite glaucony indicates Mg-rich Precambrian ocean. SiO_2 content in Lower quartzite glaucony varies from 46.42 to 57.14 wt%. This SiO_2 in Lower quartzite glaucony is similar to other glaucony bed in Vindhyan basin (Banerjee et al., 2008) and other basin (Guimaraes et al., 2000, Ivanovskaya et al., 2006, Tang et al., 2017) as well. The negative correlation of Si versus Al in tetrahedral site infers some Si has substituted in tetrahedral site by Al. In octahedral site of Lower quartzite glaucony, Al present majority, which varies from 1.58 to 1.13 and Mg, varies from 0.39 to 0.22. Fe⁺³ cations in octahedral sites is in low concentration compare to Fe⁺². Fe⁺² varies from 0.32 to 0.14, and Fe⁺³ from 0.23 to 0.10. Total octahedral in R⁺³ states varies from 1.81 to 1.22 atoms, with an average value 1.52 atoms. The average Si and Al content in tetrahedral sites are 3.60 and 0.40

atoms. The cross plot of Fe/sum of octahedral charges verses $M^+/4Si$ ($M^+=$ interlayer cations) show most of the Lower quartzite glaucony are in the field of Fe-illite and Fe-Al smectite. The formula of glaucony has represented in table 2. The average formula of glaucony is as follow: $(K_{0.66} Na_{0.04} Ca_{0.02})_{0.72} (Mg_{0.31} Fe^{+2}_{0.23} Fe^{+3}_{0.16} Al_{1.35})_{2.05} (Al_{0.40} Si_{3.60})_4 O_{10} (OH)_2 .n H_2O$.

Table 1.Oxide weight percentage of glaucony in Lower quartzite, Kaimur Formation.

| Sample No. | Na ₂ O | MgO | Al ₂ O ₃ | SiO ₂ | P ₂ O ₅ | K ₂ O | CaO | TiO ₂ | MnO | Fe ₂ O ₃ | Total |
|------------------------|-------------------|------|--------------------------------|------------------|-------------------------------|------------------|------|------------------|------|--------------------------------|-------|
| Evolved ferric illites | | | | | | | | | | | |
| GK9 | 0.05 | 2.78 | 21.36 | 50.29 | 0.03 | 7.03 | 0.41 | 0.04 | 0.00 | 5.44 | 87.41 |
| | 0.05 | 3.25 | 20.38 | 53.03 | 0.03 | 7.32 | 0.41 | 0.03 | 0.01 | 4.85 | 89.36 |
| | 0.02 | 3.28 | 19.05 | 52.51 | 0.02 | 7.50 | 0.41 | 0.08 | 0.00 | 5.41 | 88.27 |
| | 0.10 | 3.07 | 18.34 | 51.81 | 0.00 | 6.93 | 0.36 | 0.04 | 0.01 | 5.29 | 85.95 |
| | 0.01 | 2.83 | 19.96 | 50.91 | 0.05 | 6.69 | 0.41 | 0.03 | 0.00 | 4.66 | 85.56 |
| | 0.06 | 3.47 | 18.90 | 55.39 | 0.00 | 7.92 | 0.41 | 0.05 | 0.00 | 6.51 | 92.71 |
| | 0.06 | 3.69 | 17.28 | 55.15 | 0.04 | 7.80 | 0.37 | 0.02 | 0.03 | 6.90 | 91.34 |
| | 0.03 | 3.54 | 18.91 | 51.14 | 0.00 | 7.27 | 0.32 | 0.04 | 0.00 | 5.23 | 86.47 |
| | 0.03 | 3.01 | 19.86 | 54.25 | 0.02 | 7.28 | 0.44 | 0.07 | 0.00 | 5.65 | 90.60 |
| | 0.05 | 3.78 | 19.63 | 54.05 | 0.01 | 7.49 | 0.40 | 0.03 | 0.00 | 4.87 | 90.30 |
| | 0.03 | 3.61 | 19.33 | 54.28 | 0.00 | 7.68 | 0.34 | 0.04 | 0.00 | 6.48 | 91.79 |
| | 0.03 | 2.96 | 21.25 | 53.51 | 0.03 | 7.25 | 0.31 | 0.03 | 0.00 | 4.65 | 90.02 |
| | 0.54 | 3.24 | 19.30 | 53.84 | 0.00 | 7.69 | 0.33 | 0.09 | 0.00 | 5.97 | 90.99 |
| | 0.00 | 2.97 | 20.93 | 51.93 | 0.01 | 7.03 | 0.34 | 0.08 | 0.00 | 4.56 | 87.86 |
| | 0.06 | 3.11 | 19.58 | 53.59 | 0.00 | 7.57 | 0.34 | 0.08 | 0.00 | 6.17 | 90.50 |
| | 0.03 | 3.39 | 18.75 | 55.20 | 0.09 | 7.36 | 0.15 | 0.10 | 0.04 | 6.30 | 91.40 |
| | 0.03 | 3.58 | 17.81 | 55.94 | 0.01 | 7.90 | 0.28 | 0.05 | 0.00 | 7.08 | 92.68 |
| | 0.03 | 3.12 | 19.24 | 53.58 | 0.01 | 7.65 | 0.32 | 0.12 | 0.00 | 5.46 | 89.52 |
| | 0.02 | 3.27 | 19.29 | 52.56 | 0.00 | 7.47 | 0.45 | 0.04 | 0.04 | 5.22 | 88.36 |
| | 0.04 | 3.32 | 18.47 | 53.43 | 0.02 | 7.64 | 0.32 | 0.00 | 0.00 | 6.10 | 89.35 |
| | 0.06 | 2.86 | 17.65 | 49.68 | 0.02 | 6.82 | 0.36 | 0.04 | 0.03 | 5.37 | 82.88 |
| GNS2 | 0.06 | 2.80 | 20.27 | 51.01 | 0.03 | 7.67 | 0.44 | 0.01 | 0.01 | 7.20 | 89.50 |
| | 0.25 | 3.31 | 21.25 | 50.35 | 0.00 | 7.26 | 0.39 | 0.06 | 0.00 | 9.60 | 92.47 |
| | 0.10 | 2.90 | 20.86 | 50.95 | 0.00 | 7.28 | 0.46 | 0.07 | 0.00 | 7.83 | 90.45 |
| | 0.13 | 3.32 | 20.79 | 53.67 | 0.00 | 7.61 | 0.37 | 0.03 | 0.00 | 6.75 | 92.67 |
| | 0.13 | 2.63 | 27.14 | 47.33 | 0.03 | 7.69 | 0.32 | 0.02 | 0.00 | 4.62 | 89.91 |
| | 0.14 | 2.95 | 23.32 | 54.83 | 0.00 | 7.86 | 0.42 | 0.03 | 0.00 | 6.07 | 95.62 |
| | 0.14 | 3.31 | 22.57 | 52.34 | 0.00 | 7.71 | 0.42 | 0.05 | 0.00 | 6.80 | 93.34 |
| | 0.17 | 3.11 | 22.06 | 54.43 | 0.03 | 7.45 | 0.39 | 0.11 | 0.01 | 7.99 | 95.74 |
| | 0.17 | 2.80 | 25.38 | 48.75 | 0.05 | 7.79 | 0.45 | 0.13 | 0.00 | 4.54 | 90.05 |
| | 0.21 | 2.83 | 19.89 | 49.15 | 0.02 | 7.67 | 0.48 | 0.02 | 0.00 | 7.25 | 87.51 |
| | 0.10 | 2.68 | 22.62 | 52.35 | 0.04 | 7.78 | 0.52 | 0.00 | 0.00 | 5.85 | 91.93 |
| | 0.04 | 2.55 | 19.45 | 53.27 | 0.08 | 7.35 | 0.56 | 0.00 | 0.00 | 7.43 | 90.74 |
| | 0.09 | 2.87 | 24.88 | 51.76 | 0.01 | 8.06 | 0.28 | 0.05 | 0.00 | 4.85 | 92.86 |
| | 0.08 | 3.27 | 19.23 | 57.14 | 0.02 | 6.93 | 0.63 | 0.03 | 0.00 | 9.07 | 96.39 |
| | 0.12 | 3.27 | 24.02 | 46.42 | 0.03 | 7.32 | 0.42 | 0.04 | 0.00 | 6.83 | 88.46 |
| | 0.14 | 3.42 | 19.76 | 55.55 | 0.00 | 7.80 | 0.16 | 0.01 | 0.00 | 9.20 | 96.03 |
| | 0.08 | 3.18 | 19.93 | 50.58 | 0.00 | 7.97 | 0.12 | 0.00 | 0.00 | 8.69 | 90.56 |
| | 0.12 | 3.38 | 23.26 | 55.40 | 0.01 | 7.92 | 0.16 | 0.02 | 0.00 | 5.16 | 95.41 |

| | | | | | | | | | | | |
|------|------|------|-------|-------|------|------|------|------|------|------|-------|
| | 0.13 | 3.42 | 23.07 | 55.73 | 0.01 | 8.20 | 0.11 | 0.00 | 0.00 | 5.27 | 95.94 |
| | 0.11 | 3.08 | 21.68 | 56.60 | 0.00 | 7.54 | 0.10 | 0.00 | 0.00 | 6.76 | 95.86 |
| | 0.09 | 3.00 | 21.71 | 55.20 | 0.00 | 7.59 | 0.11 | 0.00 | 0.00 | 6.59 | 94.29 |
| GNS4 | 0.14 | 3.08 | 22.28 | 54.01 | 0.01 | 8.14 | 0.09 | 0.02 | 0.00 | 7.31 | 95.09 |
| | 0.09 | 3.57 | 21.04 | 55.17 | 0.01 | 7.93 | 0.11 | 0.00 | 0.00 | 6.66 | 94.56 |
| | 0.17 | 3.36 | 21.04 | 55.16 | 0.03 | 7.87 | 0.16 | 0.00 | 0.00 | 7.46 | 95.24 |
| | 0.13 | 3.85 | 20.54 | 55.81 | 0.00 | 7.99 | 0.16 | 0.00 | 0.00 | 7.23 | 95.71 |
| | 0.09 | 3.76 | 21.23 | 55.36 | 0.01 | 7.91 | 0.09 | 0.00 | 0.00 | 6.57 | 95.04 |
| | 0.13 | 3.07 | 23.17 | 55.72 | 0.00 | 7.97 | 0.14 | 0.00 | 0.00 | 6.45 | 96.65 |
| | 0.11 | 3.26 | 23.25 | 54.62 | 0.01 | 8.08 | 0.16 | 0.00 | 0.00 | 5.99 | 95.47 |
| | 0.15 | 3.29 | 22.71 | 54.56 | 0.01 | 8.11 | 0.13 | 0.00 | 0.00 | 6.01 | 94.97 |
| | 0.15 | 2.97 | 24.21 | 54.82 | 0.00 | 8.14 | 0.06 | 0.00 | 0.00 | 5.53 | 95.90 |
| | 0.08 | 3.59 | 19.18 | 54.49 | 0.00 | 7.64 | 0.13 | 0.00 | 0.00 | 8.95 | 94.07 |
| | 0.10 | 3.15 | 22.09 | 54.86 | 0.00 | 7.76 | 0.16 | 0.02 | 0.00 | 6.66 | 94.80 |
| | 0.09 | 2.79 | 24.77 | 54.43 | 0.02 | 7.97 | 0.15 | 0.00 | 0.00 | 4.51 | 94.72 |
| | 0.06 | 2.69 | 21.48 | 51.58 | 0.01 | 7.01 | 0.13 | 0.00 | 0.00 | 7.08 | 90.04 |
| | 0.06 | 2.72 | 21.29 | 49.54 | 0.00 | 7.02 | 0.13 | 0.00 | 0.00 | 4.77 | 85.54 |
| | 0.05 | 2.83 | 20.31 | 52.08 | 0.00 | 7.19 | 0.01 | 0.02 | 0.00 | 6.99 | 89.46 |
| | 0.16 | 3.51 | 19.80 | 55.13 | 0.01 | 7.87 | 0.14 | 0.00 | 0.00 | 8.19 | 94.81 |
| | 0.13 | 2.96 | 22.47 | 56.18 | 0.01 | 7.65 | 0.13 | 0.00 | 0.00 | 6.51 | 96.04 |
| | 0.16 | 3.10 | 22.79 | 55.70 | 0.00 | 7.94 | 0.15 | 0.00 | 0.00 | 6.47 | 96.31 |
| GNS7 | 0.06 | 3.76 | 21.16 | 54.25 | 0.00 | 7.54 | 0.32 | 0.00 | 0.05 | 6.99 | 94.13 |
| | 0.01 | 3.83 | 20.43 | 55.84 | 0.00 | 8.00 | 0.32 | 0.06 | 0.00 | 8.40 | 96.88 |
| | 0.06 | 3.38 | 20.87 | 55.17 | 0.00 | 8.23 | 0.25 | 0.05 | 0.00 | 7.32 | 95.33 |
| | 0.01 | 3.49 | 23.41 | 53.67 | 0.00 | 7.77 | 0.38 | 0.04 | 0.02 | 7.53 | 96.32 |
| | 0.05 | 3.18 | 26.76 | 53.74 | 0.01 | 8.27 | 0.35 | 0.01 | 0.00 | 4.50 | 96.87 |
| | 0.08 | 2.90 | 16.94 | 56.17 | 0.01 | 7.68 | 0.36 | 0.08 | 0.00 | 8.26 | 92.48 |
| | 0.05 | 2.56 | 19.80 | 47.81 | 0.00 | 7.72 | 0.35 | 0.06 | 0.00 | 7.00 | 85.36 |
| | 0.03 | 2.88 | 27.68 | 50.33 | 0.00 | 7.64 | 0.26 | 0.00 | 0.00 | 4.99 | 93.80 |
| | 0.06 | 2.18 | 19.18 | 56.60 | 0.00 | 7.14 | 0.29 | 0.07 | 0.02 | 5.94 | 91.48 |
| | 0.07 | 3.68 | 15.98 | 52.65 | 0.08 | 7.59 | 0.29 | 0.05 | 0.00 | 9.52 | 89.91 |
| | 0.10 | 3.11 | 23.85 | 53.07 | 0.00 | 7.78 | 0.32 | 0.17 | 0.03 | 5.44 | 93.87 |
| | 0.03 | 3.71 | 21.19 | 56.24 | 0.00 | 7.49 | 0.28 | 0.09 | 0.01 | 7.35 | 96.39 |
| Max. | 0.54 | 3.85 | 27.68 | 57.14 | 0.09 | 8.27 | 0.63 | 0.17 | 0.05 | 9.60 | 96.88 |
| Min. | 0.00 | 2.18 | 15.98 | 46.42 | 0.00 | 6.69 | 0.01 | 0.00 | 0.00 | 4.50 | 82.88 |
| Mean | 0.27 | 3.02 | 21.83 | 51.78 | 0.04 | 7.48 | 0.32 | 0.09 | 0.03 | 7.05 | 89.88 |

Table 2 Structural composition of glaucony in Lower quartzite, Kaimur Formation.

| Sample No. | Structural Formulae Of Fully evolved ferric illites | Tetrahedral charge | Octahedral charge |
|------------|--|--------------------|-------------------|
| GK9 | (K _{0.65} ,Na _{0.01} , Ca _{0.03}) _{0.68} (Mg _{0.30} ,Fe ⁺³ _{0.13} ,Fe ⁺² _{0.18} , Al _{1.44}) _{2.05} (Al _{0.38} ,Si _{3.62}) ₄ O ₁₁ (OH) ₂ .nH ₂ O | 0.38 | 0.17 |
| | (K _{0.66} ,Na _{0.01} , Ca _{0.03}) _{0.69} (Mg _{0.34} ,Fe ⁺³ _{0.10} ,Fe ⁺² _{0.14} , Al _{1.43}) _{2.02} (Al _{0.28} ,Si _{3.72}) ₄ O ₁₁ (OH) ₂ .nH ₂ O | 0.28 | 0.20 |
| | (K _{0.68} ,Na _{0.00} , Ca _{0.03}) _{0.71} (Mg _{0.33} ,Fe ⁺³ _{0.13} ,Fe ⁺² _{0.18} , Al _{1.35}) _{2.01} (Al _{0.25} ,Si _{3.7}) ₄ O ₁₁ (OH) ₂ .nH ₂ O | 0.25 | 0.21 |
| | (K _{0.65} ,Na _{0.01} , Ca _{0.03}) _{0.69} (Mg _{0.33} ,Fe ⁺³ _{0.13} ,Fe ⁺² _{0.18} , Al _{1.36}) _{2.01} (Al _{0.22} ,Si _{3.78}) ₄ O ₁₁ (OH) ₂ .nH ₂ O | 0.22 | 0.20 |
| | (K _{0.62} ,Na _{0.00} , Ca _{0.03}) _{0.65} (Mg _{0.31} ,Fe ⁺³ _{0.11} ,Fe ⁺² _{0.16} , Al _{1.36}) _{2.02} (Al _{0.28} ,Si _{3.72}) ₄ O ₁₁ (OH) ₂ .nH ₂ O | 0.28 | 0.18 |
| | (K _{0.69} ,Na _{0.01} , Ca _{0.03}) _{0.73} (Mg _{0.35} ,Fe ⁺³ _{0.15} ,Fe ⁺² _{0.21} , Al _{1.30}) _{2.01} (Al _{0.22} ,Si _{3.78}) ₄ O ₁₁ (OH) ₂ .nH ₂ O | 0.22 | 0.21 |
| | (K _{0.69} ,Na _{0.01} , Ca _{0.03}) _{0.72} (Mg _{0.38} ,Fe ⁺³ _{0.16} ,Fe ⁺² _{0.22} , Al _{1.24}) _{2.01} (Al _{0.17} ,Si _{3.83}) ₄ O ₁₁ (OH) ₂ .nH ₂ O | 0.17 | 0.22 |
| | (K _{0.68} ,Na _{0.00} , Ca _{0.02}) _{0.70} (Mg _{0.38} ,Fe ⁺³ _{0.13} ,Fe ⁺² _{0.18} , Al _{1.35}) _{2.04} (Al _{0.28} ,Si _{3.72}) ₄ O ₁₁ (OH) ₂ .nH ₂ O | 0.28 | 0.23 |
| | (K _{0.64} ,Na _{0.00} , Ca _{0.03}) _{0.67} (Mg _{0.31} ,Fe ⁺³ _{0.14} ,Fe ⁺² _{0.18} , Al _{1.38}) _{2.01} (Al _{0.24} ,Si _{3.76}) ₄ O ₁₁ (OH) ₂ .nH ₂ O | 0.24 | 0.18 |
| | (K _{0.66} ,Na _{0.01} , Ca _{0.03}) _{0.70} (Mg _{0.39} ,Fe ⁺³ _{0.11} ,Fe ⁺² _{0.16} , Al _{1.36}) _{2.02} (Al _{0.25} ,Si _{3.75}) ₄ O ₁₁ (OH) ₂ .nH ₂ O | 0.25 | 0.24 |
| | (K _{0.67} ,Na _{0.00} , Ca _{0.03}) _{0.70} (Mg _{0.37} ,Fe ⁺³ _{0.15} ,Fe ⁺² _{0.21} , Al _{1.31}) _{2.04} (Al _{0.26} ,Si _{3.74}) ₄ O ₁₁ (OH) ₂ .nH ₂ O | 0.26 | 0.22 |
| | (K _{0.66} ,Na _{0.00} , Ca _{0.02}) _{0.67} (Mg _{0.31} ,Fe ⁺³ _{0.11} ,Fe ⁺² _{0.15} , Al _{1.45}) _{2.02} (Al _{0.29} ,Si _{3.71}) ₄ O ₁₁ (OH) ₂ .nH ₂ O | 0.29 | 0.18 |
| | (K _{0.68} ,Na _{0.07} , Ca _{0.02}) _{0.77} (Mg _{0.34} ,Fe ⁺³ _{0.14} ,Fe ⁺² _{0.19} , Al _{1.33}) _{2.00} (Al _{0.26} ,Si _{3.75}) ₄ O ₁₁ (OH) ₂ .nH ₂ O | 0.25 | 0.20 |
| | (K _{0.64} Na _{0.00} , Ca _{0.03}) _{0.67} (Mg _{0.32} ,Fe ⁺³ _{0.11} ,Fe ⁺² _{0.15} , Al _{1.45}) _{2.03} (Al _{0.30} ,Si _{3.70}) ₄ O ₁₁ (OH) ₂ .nH ₂ O | 0.30 | 0.18 |
| | (K _{0.67} ,Na _{0.01} , Ca _{0.03}) _{0.71} (Mg _{0.32} ,Fe ⁺³ _{0.14} ,Fe ⁺² _{0.20} , Al _{1.35}) _{2.02} (Al _{0.26} ,Si _{3.74}) ₄ O ₁₁ (OH) ₂ .nH ₂ O | 0.26 | 0.19 |
| | (K _{0.65} ,Na _{0.00} , Ca _{0.01}) _{0.66} (Mg _{0.35} ,Fe ⁺³ _{0.15} ,Fe ⁺² _{0.20} , Al _{1.33}) _{2.03} (Al _{0.20} ,Si _{3.80}) ₄ O ₁₁ (OH) ₂ .nH ₂ O | 0.20 | 0.21 |
| | (K _{0.69} ,Na _{0.00} , Ca _{0.02}) _{0.71} (Mg _{0.36} ,Fe ⁺³ _{0.16} ,Fe ⁺² _{0.22} , Al _{1.26}) _{2.01} (Al _{0.18} ,Si _{3.82}) ₄ O ₁₁ (OH) ₂ .nH ₂ O | 0.18 | 0.22 |
| | (K _{0.69} ,Na _{0.00} , Ca _{0.02}) _{0.71} (Mg _{0.33} ,Fe ⁺³ _{0.13} ,Fe ⁺² _{0.18} , Al _{1.37}) _{2.01} (Al _{0.23} ,Si _{3.77}) ₄ O ₁₁ (OH) ₂ .nH ₂ O | 0.23 | 0.22 |
| | (K _{0.68} ,Na _{0.00} ,Ca _{0.03}) _{0.71} (Mg _{0.35} ,Fe ⁺³ _{0.12} ,Fe ⁺² _{0.17} , Al _{1.36}) _{2.01} (Al _{0.26} ,Si _{3.74}) ₄ O ₁₁ (OH) ₂ .nH ₂ O | 0.26 | 0.21 |
| | (K _{0.69} ,Na _{0.01} , Ca _{0.02}) _{0.72} (Mg _{0.35} ,Fe ⁺³ _{0.14} ,Fe ⁺² _{0.20} , Al _{1.32}) _{2.01} (Al _{0.22} ,Si _{3.78}) ₄ O ₁₁ (OH) ₂ .nH ₂ O | 0.22 | 0.21 |
| | (K _{0.66} ,Na _{0.01} , Ca _{0.03}) _{0.70} (Mg _{0.32} ,Fe ⁺³ _{0.14} ,Fe ⁺² _{0.19} , Al _{1.35}) _{2.01} (Al _{0.23} ,Si _{3.77}) ₄ O ₁₁ (OH) ₂ .nH ₂ O | 0.23 | 0.19 |
| | (K _{0.70} ,Na _{0.01} , Ca _{0.03}) _{0.74} (Mg _{0.30} ,Fe ⁺³ _{0.17} ,Fe ⁺² _{0.24} , Al _{1.34}) _{2.04} | 0.37 | 0.17 |

| | | | |
|------|---|------|------|
| GNS2 | (Al _{0.37} ,Si _{3.63}) ₄ O ₁₁ (OH) ₂ .nH ₂ O | | |
| | (K _{0.65} ,Na _{0.03} , Ca _{0.03}) _{0.71} (Mg _{0.34} ,Fe ⁺³ _{0.22} ,Fe ⁺² _{0.31} , Al _{1.26}) _{2.14} (Al _{0.49} ,Si _{3.51}) ₄ O ₁₁ (OH) ₂ .nH ₂ O | 0.49 | 0.19 |
| | (K _{0.66} ,Na _{0.01} , Ca _{0.03}) _{0.70} (Mg _{0.31} ,Fe ⁺³ _{0.18} ,Fe ⁺² _{0.26} , Al _{1.33}) _{2.08} (Al _{0.40} ,Si _{3.60}) ₄ O ₁₁ (OH) ₂ .nH ₂ O | 0.40 | 0.17 |
| | (K _{0.66} ,Na _{0.02} , Ca _{0.03}) _{0.71} (Mg _{0.34} ,Fe ⁺³ _{0.15} ,Fe ⁺² _{0.21} , Al _{1.35}) _{2.05} (Al _{0.33} ,Si _{3.67}) ₄ O ₁₁ (OH) ₂ .nH ₂ O | 0.33 | 0.20 |
| | (K _{0.69} ,Na _{0.02} , Ca _{0.02}) _{0.73} (Mg _{0.28} ,Fe ⁺³ _{0.11} ,Fe ⁺² _{0.15} , Al _{1.58}) _{2.12} (Al _{0.67} ,Si _{3.33}) ₄ O ₁₁ (OH) ₂ .nH ₂ O | 0.67 | 0.15 |
| | (K _{0.66} ,Na _{0.02} , Ca _{0.03}) _{0.71} (Mg _{0.29} ,Fe ⁺³ _{0.13} ,Fe ⁺² _{0.19} , Al _{1.43}) _{2.04} (Al _{0.38} ,Si _{3.62}) ₄ O ₁₁ (OH) ₂ .nH ₂ O | 0.38 | 0.17 |
| | (K _{0.67} ,Na _{0.02} , Ca _{0.03}) _{0.72} (Mg _{0.31} ,Fe ⁺³ _{0.15} ,Fe ⁺² _{0.22} , Al _{1.38}) _{2.08} (Al _{0.44} ,Si _{3.56}) ₄ O ₁₁ (OH) ₂ .nH ₂ O | 0.44 | 0.19 |
| | (K _{0.63} ,Na _{0.02} , Ca _{0.03}) _{0.68} (Mg _{0.34} ,Fe ⁺³ _{0.18} ,Fe ⁺² _{0.25} , Al _{1.35}) _{2.08} (Al _{0.38} ,Si _{3.62}) ₄ O ₁₁ (OH) ₂ .nH ₂ O | 0.38 | 0.17 |
| | (K _{0.70} ,Na _{0.02} , Ca _{0.03}) _{0.75} (Mg _{0.29} ,Fe ⁺³ _{0.11} ,Fe ⁺² _{0.15} , Al _{1.53}) _{2.08} (Al _{0.57} ,Si _{3.43}) ₄ O ₁₁ (OH) ₂ .nH ₂ O | 0.57 | 0.16 |
| | (K _{0.72} ,Na _{0.03} , Ca _{0.04}) _{0.79} (Mg _{0.31} ,Fe ⁺³ _{0.18} ,Fe ⁺² _{0.25} , Al _{1.32}) _{2.05} (Al _{0.40} ,Si _{3.60}) ₄ O ₁₁ (OH) ₂ .nH ₂ O | 0.40 | 0.18 |
| | (K _{0.68} ,Na _{0.01} , Ca _{0.04}) _{0.74} (Mg _{0.27} ,Fe ⁺³ _{0.13} ,Fe ⁺² _{0.19} , Al _{1.44}) _{2.03} (Al _{0.40} ,Si _{3.60}) ₄ O ₁₁ (OH) ₂ .nH ₂ O | 0.40 | 0.16 |
| | (K _{0.66} ,Na _{0.01} , Ca _{0.04}) _{0.71} (Mg _{0.27} ,Fe ⁺³ _{0.17} ,Fe ⁺² _{0.24} , Al _{1.33}) _{2.01} (Al _{0.27} ,Si _{3.73}) ₄ O ₁₁ (OH) ₂ .nH ₂ O | 0.27 | 0.15 |
| | (K _{0.70} ,Na _{0.01} , Ca _{0.02}) _{0.73} (Mg _{0.29} ,Fe ⁺³ _{0.11} ,Fe ⁺² _{0.15} , Al _{1.51}) _{2.06} (Al _{0.48} ,Si _{3.52}) ₄ O ₁₁ (OH) ₂ .nH ₂ O | 0.48 | 0.16 |
| | (K _{0.58} ,Na _{0.01} , Ca _{0.04}) _{0.63} (Mg _{0.32} ,Fe ⁺³ _{0.20} ,Fe ⁺² _{0.28} , Al _{1.26}) _{2.05} (Al _{0.24} ,Si _{3.76}) ₄ O ₁₁ (OH) ₂ .nH ₂ O | 0.24 | 0.18 |
| | (K _{0.68} ,Na _{0.02} , Ca _{0.03}) _{0.73} (Mg _{0.35} ,Fe ⁺³ _{0.17} ,Fe ⁺² _{0.23} , Al _{1.41}) _{2.16} (Al _{0.64} ,Si _{3.36}) ₄ O ₁₁ (OH) ₂ .nH ₂ O | 0.64 | 0.20 |
| | (K _{0.66} ,Na _{0.02} , Ca _{0.01}) _{0.69} (Mg _{0.34} ,Fe ⁺³ _{0.20} ,Fe ⁺² _{0.28} , Al _{1.25}) _{2.08} (Al _{0.30} ,Si _{3.70}) ₄ O ₁₁ (OH) ₂ .nH ₂ O | 0.30 | 0.20 |
| | (K _{0.72} ,Na _{0.01} , Ca _{0.01}) _{0.74} (Mg _{0.34} ,Fe ⁺³ _{0.21} ,Fe ⁺² _{0.29} , Al _{1.26}) _{2.09} (Al _{0.41} ,Si _{3.59}) ₄ O ₁₁ (OH) ₂ .nH ₂ O | 0.41 | 0.19 |
| | (K _{0.66} ,Na _{0.2} , Ca _{0.01}) _{0.69} (Mg _{0.33} ,Fe ⁺³ _{0.11} ,Fe ⁺² _{0.16} , Al _{1.45}) _{2.05} (Al _{0.36} ,Si _{3.64}) ₄ O ₁₁ (OH) ₂ .nH ₂ O | 0.36 | 0.19 |
| | (K _{0.69} ,Na _{0.02} , Ca _{0.01}) _{0.72} (Mg _{0.33} ,Fe ⁺³ _{0.12} ,Fe ⁺² _{0.16} , Al _{1.43}) _{2.04} (Al _{0.35} ,Si _{3.65}) ₄ O ₁₁ (OH) ₂ .nH ₂ O | 0.35 | 0.20 |
| | (K _{0.63} ,Na _{0.01} , Ca _{0.01}) _{0.65} (Mg _{0.30} ,Fe ⁺³ _{0.15} ,Fe ⁺² _{0.21} , Al _{1.39}) _{2.05} (Al _{0.29} ,Si _{3.71}) ₄ O ₁₁ (OH) ₂ .nH ₂ O | 0.29 | 0.17 |
| | (K _{0.65} ,Na _{0.01} , Ca _{0.01}) _{0.67} (Mg _{0.30} ,Fe ⁺³ _{0.15} ,Fe ⁺² _{0.20} , Al _{1.40}) _{2.05} (Al _{0.31} ,Si _{3.69}) ₄ O ₁₁ (OH) ₂ .nH ₂ O | 0.31 | 0.17 |
| | (K _{0.63} ,Na _{0.02} , Ca _{0.01}) _{0.66} (Mg _{0.32} ,Fe ⁺³ _{0.18} ,Fe ⁺² _{0.25} , Al _{1.33}) _{2.08} (Al _{0.32} ,Si _{3.68}) ₄ O ₁₁ (OH) ₂ .nH ₂ O | 0.32 | 0.18 |
| | (K _{0.69} ,Na _{0.02} , Ca _{0.01}) _{0.72} (Mg _{0.31} ,Fe ⁺³ _{0.16} ,Fe ⁺² _{0.23} , Al _{1.37}) _{2.07} (Al _{0.39} ,Si _{3.61}) ₄ O ₁₁ (OH) ₂ .nH ₂ O | 0.39 | 0.17 |
| | (K _{0.68} ,Na _{0.01} , Ca _{0.01}) _{0.70} (Mg _{0.36} ,Fe ⁺³ _{0.15} ,Fe ⁺² _{0.21} , Al _{1.35}) _{2.06} (Al _{0.31} ,Si _{3.69}) ₄ O ₁₁ (OH) ₂ .nH ₂ O | 0.31 | 0.21 |
| | (K _{0.67} ,Na _{0.02} , Ca _{0.03}) _{0.72} (Mg _{0.33} ,Fe ⁺³ _{0.17} ,Fe ⁺² _{0.23} , Al _{1.33}) _{2.06} (Al _{0.32} ,Si _{3.68}) ₄ O ₁₁ (OH) ₂ .nH ₂ O | 0.32 | 0.19 |
| | | | |
| | | | |
| | | | |
| | | | |
| | | | |
| | | | |

| | | | |
|------|---|------|------|
| | (K _{0.68} ,Na _{0.02} ,Ca _{0.01}) _{0.71} (Mg _{0.38} ,Fe ⁺³ _{0.16} ,Fe ⁺² _{0.22} ,Al _{1.30}) _{2.07} (Al _{0.30} ,Si _{3.70}) ₄ O ₁₁ (OH) ₂ .nH ₂ O | 0.30 | 0.23 |
| | (K _{0.67} ,Na _{0.01} ,Ca _{0.01}) _{0.69} (Mg _{0.37} ,Fe ⁺³ _{0.15} ,Fe ⁺² _{0.20} ,Al _{1.35}) _{2.07} (Al _{0.32} ,Si _{3.68}) ₄ O ₁₁ (OH) ₂ .nH ₂ O | 0.32 | 0.22 |
| | (K _{0.66} ,Na _{0.02} ,Ca _{0.01}) _{0.69} (Mg _{0.30} ,Fe ⁺³ _{0.14} ,Fe ⁺² _{0.20} ,Al _{1.42}) _{2.06} (Al _{0.36} ,Si _{3.64}) ₄ O ₁₁ (OH) ₂ .nH ₂ O | 0.36 | 0.17 |
| | (K _{0.68} ,Na _{0.01} ,Ca _{0.01}) _{0.70} (Mg _{0.32} ,Fe ⁺³ _{0.13} ,Fe ⁺² _{0.18} ,Al _{1.42}) _{2.06} (Al _{0.39} ,Si _{3.61}) ₄ O ₁₁ (OH) ₂ .nH ₂ O | 0.39 | 0.18 |
| | (K _{0.69} ,Na _{0.02} ,Ca _{0.01}) _{0.72} (Mg _{0.33} ,Fe ⁺³ _{0.13} ,Fe ⁺² _{0.19} ,Al _{1.41}) _{2.06} (Al _{0.37} ,Si _{3.63}) ₄ O ₁₁ (OH) ₂ .nH ₂ O | 0.37 | 0.19 |
| | (K _{0.68} ,Na _{0.02} ,Ca _{0.00}) _{0.70} (Mg _{0.29} ,Fe ⁺³ _{0.12} ,Fe ⁺² _{0.17} ,Al _{1.47}) _{2.05} (Al _{0.40} ,Si _{3.60}) ₄ O ₁₁ (OH) ₂ .nH ₂ O | 0.40 | 0.17 |
| | (K _{0.66} ,Na _{0.01} ,Ca _{0.01}) _{0.68} (Mg _{0.36} ,Fe ⁺³ _{0.20} ,Fe ⁺² _{0.28} ,Al _{1.24}) _{2.09} (Al _{0.30} ,Si _{3.70}) ₄ O ₁₁ (OH) ₂ .nH ₂ O | 0.30 | 0.21 |
| | (K _{0.66} ,Na _{0.01} ,Ca _{0.01}) _{0.68} (Mg _{0.31} ,Fe ⁺³ _{0.15} ,Fe ⁺² _{0.21} ,Al _{1.39}) _{2.05} (Al _{0.34} ,Si _{3.66}) ₄ O ₁₁ (OH) ₂ .nH ₂ O | 0.34 | 0.18 |
| | (K _{0.67} ,Na _{0.01} ,Ca _{0.01}) _{0.69} (Mg _{0.27} ,Fe ⁺³ _{0.10} ,Fe ⁺² _{0.14} ,Al _{1.53}) _{2.04} (Al _{0.40} ,Si _{3.60}) ₄ O ₁₁ (OH) ₂ .nH ₂ O | 0.40 | 0.16 |
| | (K _{0.63} ,Na _{0.01} ,Ca _{0.01}) _{0.65} (Mg _{0.28} ,Fe ⁺³ _{0.17} ,Fe ⁺² _{0.23} ,Al _{1.40}) _{2.08} (Al _{0.38} ,Si _{3.62}) ₄ O ₁₁ (OH) ₂ .nH ₂ O | 0.38 | 0.16 |
| | (K _{0.66} ,Na _{0.01} ,Ca _{0.01}) _{0.68} (Mg _{0.30} ,Fe ⁺³ _{0.12} ,Fe ⁺² _{0.16} ,Al _{1.47}) _{2.05} (Al _{0.37} ,Si _{3.63}) ₄ O ₁₁ (OH) ₂ .nH ₂ O | 0.37 | 0.17 |
| | (K _{0.65} ,Na _{0.01} ,Ca _{0.00}) _{0.66} (Mg _{0.30} ,Fe ⁺³ _{0.17} ,Fe ⁺² _{0.23} ,Al _{1.37}) _{2.06} (Al _{0.32} ,Si _{3.68}) ₄ O ₁₁ (OH) ₂ .nH ₂ O | 0.32 | 0.17 |
| | (K _{0.67} ,Na _{0.02} ,Ca _{0.01}) _{0.70} (Mg _{0.35} ,Fe ⁺³ _{0.18} ,Fe ⁺² _{0.26} ,Al _{1.27}) _{2.07} (Al _{0.29} ,Si _{3.71}) ₄ O ₁₁ (OH) ₂ .nH ₂ O | 0.29 | 0.21 |
| | (K _{0.64} ,Na _{0.02} ,Ca _{0.01}) _{0.67} (Mg _{0.29} ,Fe ⁺³ _{0.14} ,Fe ⁺² _{0.20} ,Al _{1.42}) _{2.05} (Al _{0.32} ,Si _{3.68}) ₄ O ₁₁ (OH) ₂ .nH ₂ O | 0.32 | 0.16 |
| | (K _{0.66} ,Na _{0.02} ,Ca _{0.01}) _{0.69} (Mg _{0.30} ,Fe ⁺³ _{0.14} ,Fe ⁺² _{0.20} ,Al _{1.41}) _{2.05} (Al _{0.35} ,Si _{3.65}) ₄ O ₁₁ (OH) ₂ .nH ₂ O | 0.35 | 0.17 |
| GNS7 | (K _{0.65} ,Na _{0.01} ,Ca _{0.02}) _{0.68} (Mg _{0.38} ,Fe ⁺³ _{0.16} ,Fe ⁺² _{0.22} ,Al _{1.33}) _{2.08} (Al _{0.35} ,Si _{3.65}) ₄ O ₁₁ (OH) ₂ .nH ₂ O | 0.35 | 0.22 |
| | (K _{0.67} ,Na _{0.00} ,Ca _{0.02}) _{0.69} (Mg _{0.38} ,Fe ⁺³ _{0.19} ,Fe ⁺² _{0.26} ,Al _{1.26}) _{2.08} (Al _{0.32} ,Si _{3.68}) ₄ O ₁₁ (OH) ₂ .nH ₂ O | 0.32 | 0.22 |
| | (K _{0.70} ,Na _{0.01} ,Ca _{0.02}) _{0.73} (Mg _{0.34} ,Fe ⁺³ _{0.16} ,Fe ⁺² _{0.23} ,Al _{1.32}) _{2.05} (Al _{0.32} ,Si _{3.68}) ₄ O ₁₁ (OH) ₂ .nH ₂ O | 0.32 | 0.20 |
| | (K _{0.65} ,Na _{0.00} ,Ca _{0.03}) _{0.68} (Mg _{0.34} ,Fe ⁺³ _{0.17} ,Fe ⁺² _{0.23} ,Al _{1.37}) _{2.11} (Al _{0.46} ,Si _{3.54}) ₄ O ₁₁ (OH) ₂ .nH ₂ O | 0.46 | 0.19 |
| | (K _{0.68} ,Na _{0.01} ,Ca _{0.02}) _{0.71} (Mg _{0.31} ,Fe ⁺³ _{0.10} ,Fe ⁺² _{0.14} ,Al _{1.53}) _{2.07} (Al _{0.51} ,Si _{3.49}) ₄ O ₁₁ (OH) ₂ .nH ₂ O | 0.51 | 0.17 |
| | (K _{0.67} ,Na _{0.01} ,Ca _{0.03}) _{0.71} (Mg _{0.30} ,Fe ⁺³ _{0.19} ,Fe ⁺² _{0.26} ,Al _{1.24}) _{1.99} (Al _{0.14} ,Si _{3.86}) ₄ O ₁₁ (OH) ₂ .nH ₂ O | 0.14 | 0.18 |
| | (K _{0.74} ,Na _{0.01} ,Ca _{0.03}) _{0.78} (Mg _{0.29} ,Fe ⁺³ _{0.18} ,Fe ⁺² _{0.24} ,Al _{1.34}) _{2.05} (Al _{0.41} ,Si _{3.59}) ₄ O ₁₁ (OH) ₂ .nH ₂ O | 0.41 | 0.16 |
| | (K _{0.65} ,Na _{0.00} ,Ca _{0.02}) _{0.67} (Mg _{0.29} ,Fe ⁺³ _{0.11} ,Fe ⁺² _{0.16} ,Al _{1.57}) _{2.12} (Al _{0.62} ,Si _{3.38}) ₄ O ₁₁ (OH) ₂ .nH ₂ O | 0.62 | 0.16 |
| | (K _{0.62} ,Na _{0.01} ,Ca _{0.02}) _{0.65} (Mg _{0.22} ,Fe ⁺³ _{0.14} ,Fe ⁺² _{0.19} ,Al _{1.41}) _{1.96} (Al _{0.13} ,Si _{3.87}) ₄ O ₁₁ (OH) ₂ .nH ₂ O | 0.13 | 0.13 |
| | (K _{0.69} ,Na _{0.01} ,Ca _{0.02}) _{0.72} (Mg _{0.39} ,Fe ⁺³ _{0.23} ,Fe ⁺² _{0.32} ,Al _{1.13}) _{2.06} | 0.23 | 0.24 |

| | | | |
|--|--|------|------|
| | $(\text{Al}_{0.23}, \text{Si}_{3.77})_4 \text{O}_{11} (\text{OH})_2 \cdot n\text{H}_2\text{O}$ | | |
| | $(\text{K}_{0.67}, \text{Na}_{0.01}, \text{Ca}_{0.02})_{0.70} (\text{Mg}_{0.31}, \text{Fe}^{+3}_{0.12}, \text{Fe}^{+2}_{0.17}, \text{Al}_{1.46})_{2.07}$ | 0.43 | 0.18 |
| | $(\text{Al}_{0.43}, \text{Si}_{3.57})_4 \text{O}_{11} (\text{OH})_2 \cdot n\text{H}_2\text{O}$ | | |
| | $(\text{K}_{0.63}, \text{Na}_{0.00}, \text{Ca}_{0.02})_{0.71} (\text{Mg}_{0.36}, \text{Fe}^{+3}_{0.16}, \text{Fe}^{+2}_{0.22}, \text{Al}_{1.33})_{2.08}$ | 0.31 | 0.21 |
| | $(\text{Al}_{0.31}, \text{Si}_{3.69})_4 \text{O}_{11} (\text{OH})_2 \cdot n\text{H}_2\text{O}$ | | |

3.4. Genesis of glaucony:

Formation of glaucony has explained by the “layer lattice theory” (Brust, 1958a, 1958b; Hower, 1961), the “verdissement theory” (Odin and Matter, 1981) and the “pseudomorphic replacement theory” (Dasgupta et al., 1990) on the basis of the cross plot of $\text{K}_2\text{O}\%$ and $\text{TFe}_2\text{O}_3\%$. The constantly high $\text{K}_2\text{O}\%$ and variable $\text{TFe}_2\text{O}_3\%$ in Proterozoic Lower quartzite glauconite is also considered with “pseudomorphic replacement” (Banerjee et al., 2015, 2016; Tang et al., 2017). The cross plot of $\text{K}_2\text{O}\%$ and $\text{TFe}_2\text{O}_3\%$ in Lower quartzite glauconite infer that glauconitization was promoted by “pseudomorphic replacement” as the $\text{TFe}_2\text{O}_3\%$ increase at constant $\text{K}_2\text{O}\%$ (Fig. 3.2a). The “pseudomorphic replacement theory” explain that the abundance of K-feldspar and quartz dissolve to supply K and Si in pore-water during glauconitization. The textural evidence of k-feldspar replacement in sub-arkose Lower quartzite also supports “pseudomorphic replacement theory”.

The Fe in lower quartzite glaucony may be driven from ferruginous sea-water. The sub-arkosic substratums of lower quartzite and K-feldspar don't have enough Fe which can provide Fe in the formation lower quartzite glaucony. Glauconitization process may be initialized from K-feldspar minerals at high K and low Fe content. The abundance supply of volcanic sediment during the deposition promotes glauconitization process (Tang et al., 2017). Present of volcano clastic sediment immediately above Lower quartzite in Bhagwar shale/ Silisified shale member (Chakraborty, 2006) infer volcanoclastic sediments was present in the sub-aerial during Lower quartzite deposition. This volcano-clastic sediment erodes from sub-aerial parts and deposits in Lower quartzite. The abundant supply of Fe by continental weathering and deposition with Lower quartzite promote from initial glaucony to evolved glaucony.

The texture and structure of glaucony minerals control the Fe and Al content (ref.). In glaucony minerals octahedral cations coordinate with six oxygen or hydroxyl units

and tetrahedral cations coordinates with four oxygen (Tang et al., 2017). Presence of high Fe^{+2} in octahedral sites generate negative charges in glaucony and this might be balance by incorporation of K cations in interlayer sites (Tang et al., 2017). But in Lower quartzite glaucony, Fe^{2+} increases at constant K cations (Fig.3.3b) so, the negative charges are not balance in octahedral site. In case of Fe^{3+} K content is also constant. Lower concentrations of Fe^{3+} compare to Fe^{2+} can't balance the negative charge in octahedral sites. This negative charge has balanced by high input of Al in octahedral site. It may be another possibility that being high concentration of Al in octahedral site is balanced by Fe^{2+} inputs. These may be the possible reason being low TFe_2O_3 and high Al_2O_3 content in Precambrian glaucony.

Modal percentages of K and Fe in glaucony infer the maturity of glaucony and simultaneous increasing of these elements are directly link with time during (Odin and Matter, 1981). In Lower quartzite glaucony, 'evolved' to 'highly evolved' glaucony does not satisfy Fe percentage with high K content. "Pseudomorphic replecent" of K-feldspar inferres system have high amount of K from its initial stage but Fe is supplied from volcano-clastic sediments . So, we can't determine the time amount to evolve the Lower quartzite glaucony from its initial stage to mature stage. The negative slope of Si and Al in tetrahedral site (Fig.3.2d) and positive slope of K verse Al in tetrahedral (Fig. 3.2e) has inferred that the negative charge in tetrahedral site due to Al substitution has equalized by positive charges of K cations.

Authigenic Lower quartzite glaucony has formed from replacement of K-feldspars by 'pseudomorphic replacement. The K feldspar and sandstone substratum play role of K, Si and Al supply of Lower quartzite glaucony. The source of Fe is the volcano-clastic sediment during Lower quartzite deposition. High Mg in Lower quartzite is an indication of Mg-rich Precambrian ocean characteristics.

3.5.Paleo redox and environment significance of glaucony origin:

Simultaneous presence of Fe^{2+} and Fe^{3+} in authigenic glaucony apple to study the paleo-redox condition of glaucony depositional ocean as Fe^{+2} deposits in anoxic condition whereas Fe^{3+} deposits in an oxic condition (Dasgupta et al., 1990, Banerjee et al., 2009, 2015, 2016a, 2016b, Bansal et al., 2017, 2018, Tang et al., 2017). Presence of Fe^{2+} and Fe^{3+} in Lower quartzite glaucony gives an opportunity to understand the Mesoproterozoic ocean redox condition during Lower quartzite

deposition. To puzzle out the paleo-redox during glauconitization of Lower quartzite, we use the redox states of Fe.

Cross plot of $\text{Fe}^{2+}/\text{Fe}^{3+}$ and $\text{Fe}^{3+}/\text{TFe}$ show lower quartzite glaucony must be precipitates below oxic zone of Mesoproterozoic ocean and in a shallow depth of anoxic zone (Fig. 3.3d). But the simultaneous increment of Fe^{3+} and Fe^{2+} at $r^2=1$ (Fig. 3.3a) infers Lower quartzite glaucony deposits at a depth where both redox state of Fe co-exists i.e. in and around the chemocline where Fe^{2+} get oxidize into Fe^{3+} .

Limitation of paleo-redox condition of sea-water and glaucony texture may control the maximum concentrations of Fe (Tang et al., 2017). Attentive amount of Fe^{2+} cations ($\text{Fe}^{2+}/\text{TFe}=58\%$) in Lower quartzite glaucony infer glaucony was deposited in reducing (anoxic) condition. At the same time presence of Fe^{3+} interpreted as oxic deposition. It is likely to deposit the Lower quartzite glaucony in and around the redoxcline of ocean (Fig. 3.4a).

Distribution of dominants facies in Lower quartzite like thick thin alternating tabular cross stratification, wave ripples, thick mud drape, tidal bundles, double mud drapes infer maximum range of deposition was in shallow water sub-tidal environment i.e. within fair weather wave base (Fig. 3.4a). The Proterozoic Vindhyan basin was a shallow water Epiric sea (Bose et al., 2001;). Low concentration of Mesoproterozoic atmospheric oxygen constrains the redoxcline in shallow depth (Canfield, 2008; Holland, 2006; Canfield, 1998). Decreasing rate of oxygen content with increasing ocean water column depth has divided the ocean redox zone into three divisions as oxic, sub-oxic and anoxic (Li et al., 2010). Fe^{2+} and Fe^{3+} both can co-exist only in the sub-oxic zone and Fe^{2+} content gradually increase with increasing sub-oxic zone depth (Fig. 8a, Tang et al., 2017). So, Lower quartzite glaucony was formed in sub-oxic zone. Higher proportion of Fe^{2+} compare to Fe^{3+} in Lower quartzite glaucony might be because of lower depth of sub-oxic zone.

3.6.Conclusion:

- a. Lower quartzite glaucony formed in ‘pseudomorphic replacement’ process i.e. by replacement of K-feldspars, reacts with pore-water and sea-water at early diagenetic stage.
- b. Lower quartzite glaucony deposited in a shallow water sub-tidal environment.

- c. The shallow water sub-tidal environment of Lower quartzite prevailed sub-oxic condition during glauconitization.
- d. The chemical composition of Lower quartzite glaucony is very much similar to other Precambrian glaucony.
- e. High content of K, Al, Si were supplied due to diagenesis of K-feldspar and quartz.
- f. High Mg of Lower quartzite glaucony indicates glaucony formed in the Mg-rich Mesoproterozoic Ocean.
- g. The Fe was supplied from volcano-clastic sediment due to continental weathering transgression submerge of the sub-aerial exposures.
- h. Maximum content of Al in octahedral site of Lower quartzite glaucony did not allow incorporating high amount of Fe in octahedral sites and that may be reason of low TFe_2O_3 in Lower quartzite glaucony and Precambrian glaucony as well.

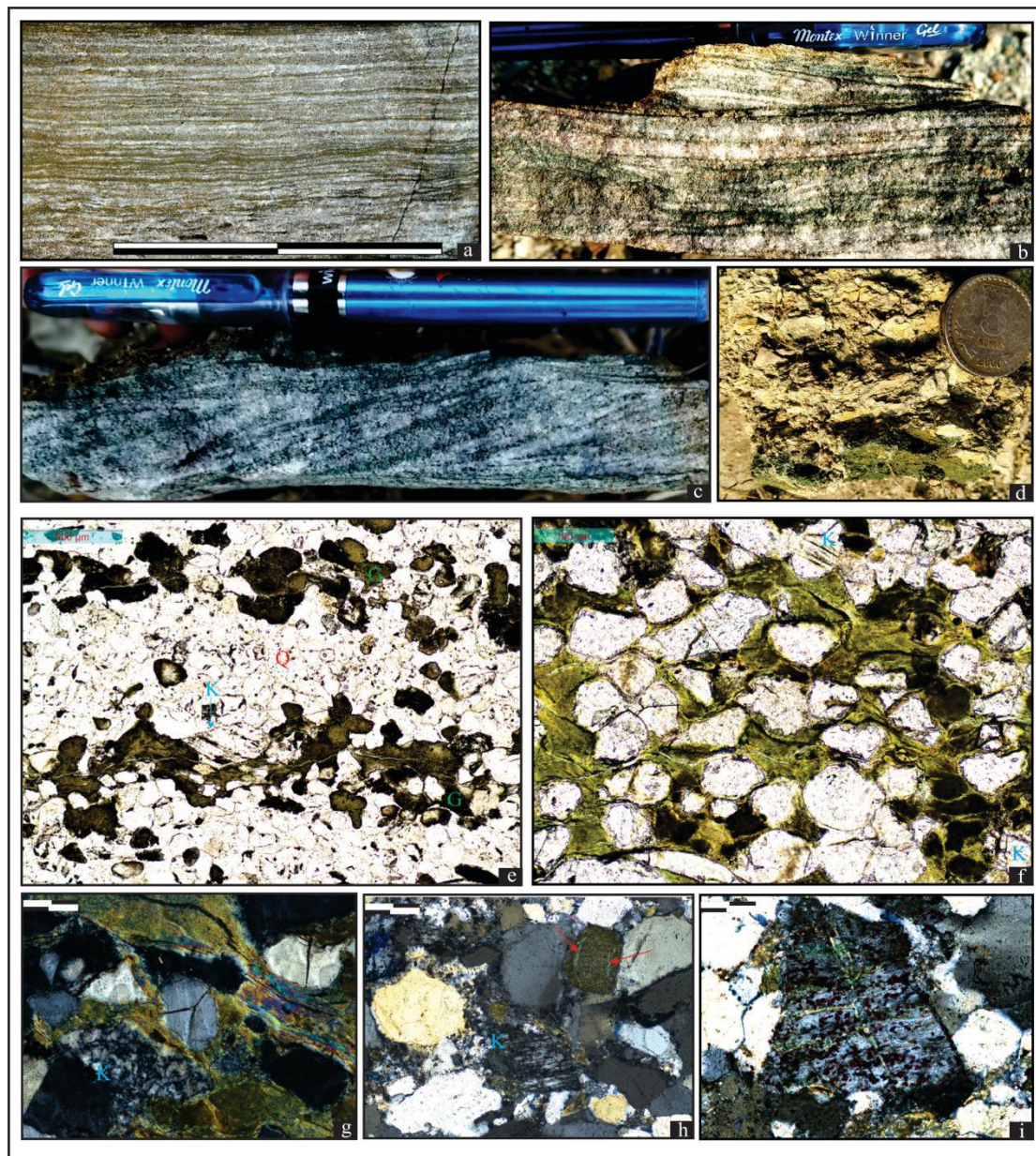


Fig. 3.1. Field photographs and the microscopic photographs of glaucony sandstone. Planer laminated glaucony sandstone (a). Ripple laminated glaucony sandstone (b and c). Planer laminated glaucony sandstone bed in lenticular fashion (d). Layer parallel origin of glaucony sandstone (e). Networking of glaucony minerals (f). Partial fulfillment of glaucony formation surrounded the feldspar grains (g) (feldspar grains has marked by k). Patchy occurrence of glaucony along the boundary of feldspar grain (h) (feldspars are marked by k) and glauconitization along the fracture plane. Glauconitization along the cleavage plane of feldspar grains (i)

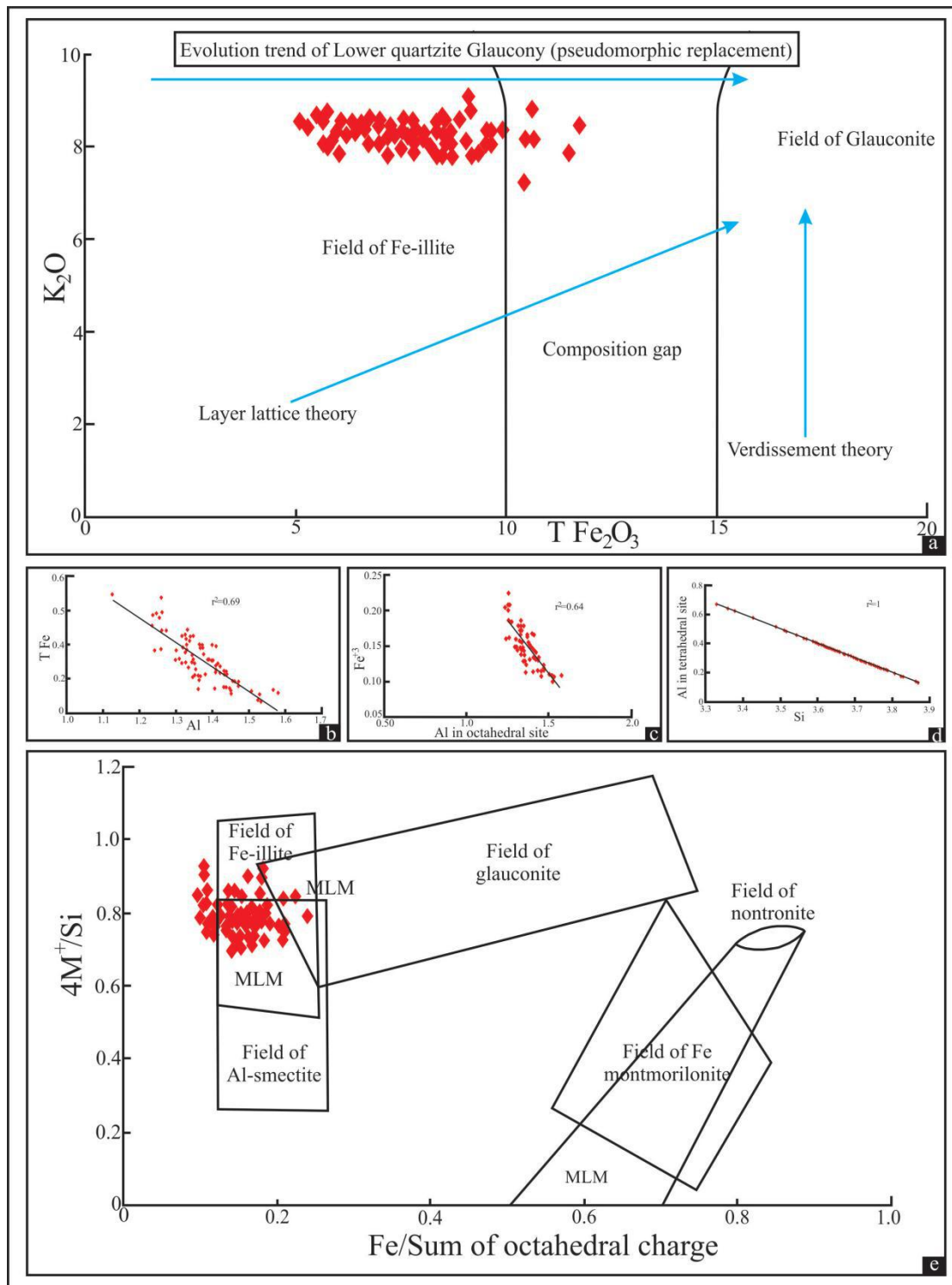


Fig. 3.2. K₂O versus TFe₂O₃ plot of glaucony mineralogy (a) (red rombs are studied glaucony sandstone). TFe versus Al plot (TFe- total iron , $r^2 = 0.69$) (b). Fe³⁺ versus Al in octahedral site plot ($r^2 = 0.64$) (c). Al in tetrahedral site versus Si plot ($r^2 = 1$) (d). Cross plot between 4M⁺/ Si (M⁺= interlayer cations) versus Fe/ sum of octahedral charge (e) (after Menuier and El Albani, 2007) (note, all data plot within the field of Fe- Illite. MLM= mixed layer minerals.

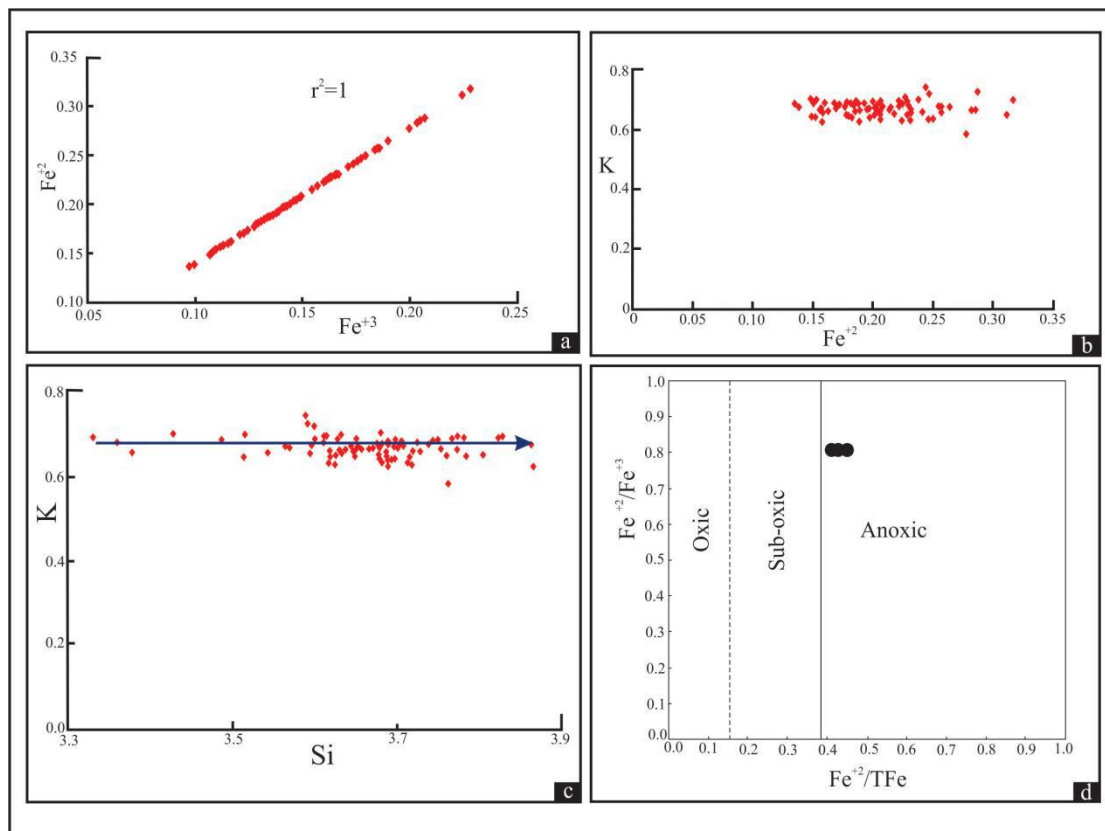


Fig 3.3 Cross plot of Fe^{2+} and Fe^{3+} ($r^2=1$) (a). Cross plot of K and Fe^{2+} (b). Cross plot of K and Si (c). Cross plot of $\text{Fe}^{2+}/\text{Fe}^{3+}$ and $\text{Fe}^{2+}/\text{TFe}$ (studied glaucony samples are within anoxic field) (d)

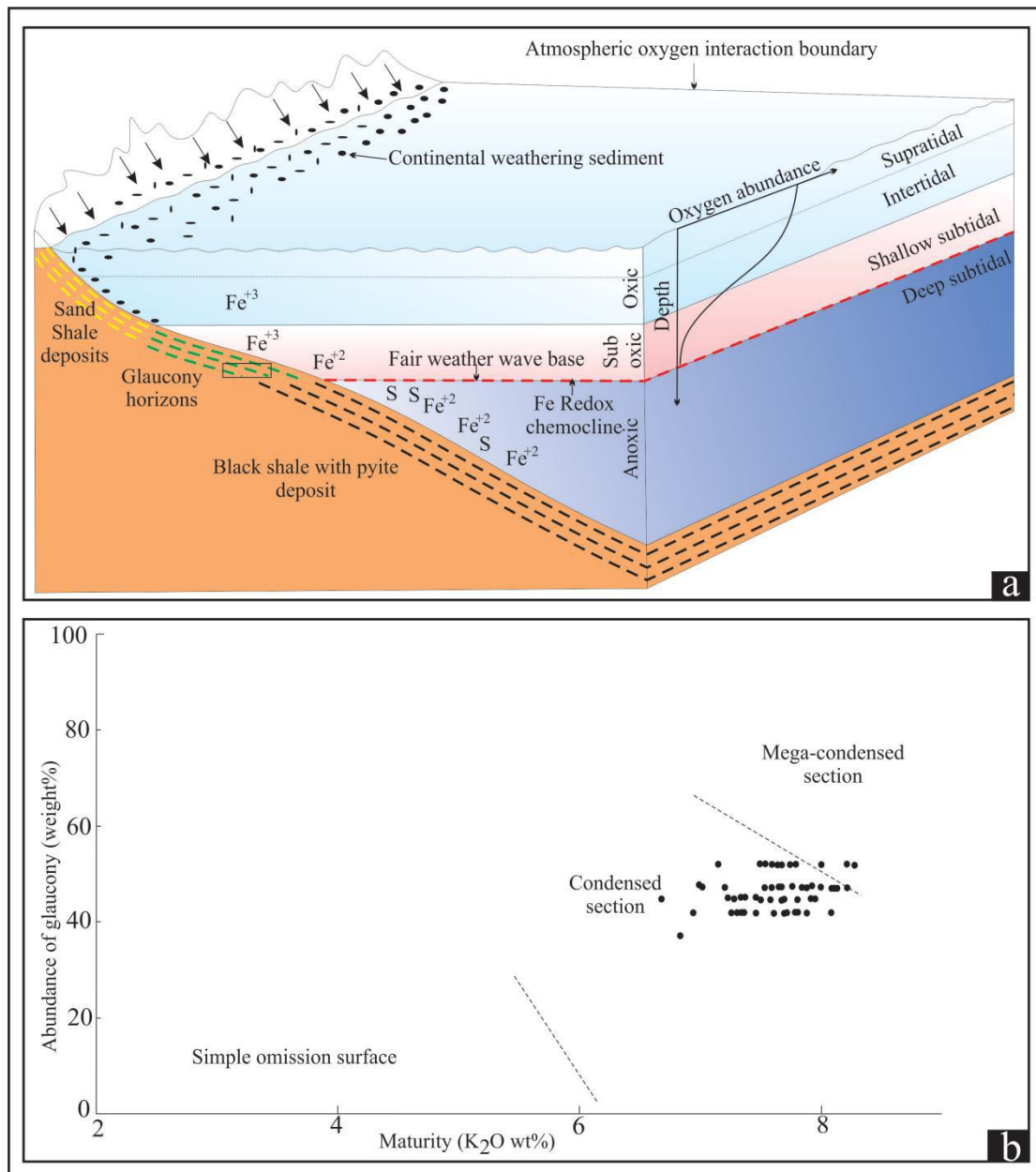


Fig 3.4. Depositional model suggested for studied glaucony sandstone (a). Relation between maturity (K₂O Wt%) and abundance of authigenic glaucony sandstone (b)

Chapter 4

Sequence building pattern of lower part of Kaimur formation

Sequence stratigraphy calls for a new outlook in stratigraphic successions. It aims for dividing a succession in genetically related stratal packages in chronologic terms, absolute or relative. Sequence stratigraphy is considered as one of the latest conceptual revolutions in the field of sedimentology revamping the methodology of stratigraphic analysis (Miall, 1995, Catuneanu et.al.,2009). The process requires prior understanding of the facies constituents. When applied to a specific depositional system, sequence stratigraphy helps to understand processes of facies formation, facies relationships, and facies cyclicity in response to base-level changes. Sequence stratigraphy is also focused on identification of key surfaces to determine the chronological order of basin filling and erosional

Demarcation of erosional boundary above Rohtas limestone (topmost member of lower vindhyan/semri group) and a thick sandstone unit on limestone deposit of Rhotas formation defines the type 1 unconformity above lower vindhyan sedimentary succession. Abundance of chertified limestone (ca 1m thick) on the top of Rohtas limestone deposit indicates a long period expose of Rohtas limestone succession (Kolondy et al. 1980).The presence of thin granular lag containing chertified limestone in between Rhotas limestone and overlying sandstone unit infer a transgressive lag deposit and this transgressive lag indicates a new episode of fresh sedimentation and emergence of sea level into the earth surface exposure.

Dominance of thick mud, herringbone cross stratified sandstone, alternating thick-thin tabular cross-stratified sandstone in lower part of sandstone deposit indicates a intertidal depositional environment. Reactivation surfaces, double mud drape in upper part is interpreted as alternating flood-ebb tidal current and intervening of slack water suspension fall out in lower tidal flat i.e. subtidal settings. Presence of hummocky cross stratification, massive beds, amalgamated thick cross stratification infer depositional site was frequently interrupted by storm action. But the overall increment of shale thickness and intertidal to subtidal transformation from lower to upper part so, a fining upward sediment succession. The fining upward sediment succession infer as a transgressive system tract deposit. The presence of glaucony horizon (ca. 60 cm) also supports the transgression system tract deposit of this studied sandstone unit.

Networking of glaucony minerals around the sand sized feldspar grains and high Mg proportion infer authigenic glauconitization in this marine settings. Presence of authigenic glaucony bed on top of this transgression system tract deposit indicates a low rate of sedimentation during glauconitization. This low rate of sedimentation also supports the transgression system tract deposit. The cross plot of abundance of glaucony versus maturity of glaucony (K_2O wt%) infer this glaucony horizon as a condense zone. But the cross stratification, ripple lamination in the association of glaucony sandstone infer the action of storm current of wave during glauconitization. The presence of Fe^{3+} along with Fe^{2+} in the octahedral site of Glaucony minerals indicates prevail of oxic condition in anoxic condense zone. The syneraxis crack, wrinkle mark in sandstone unit infer high growth of micro biota in depositional site. Presence of microbiota indicates within photic zone deposition. the condense zone of glaucony deposition is restricted within deeper part of subtidal environment (see fig 5.9 a). So this glaucony horizon may define as a flooding zone during transgression but not as a maximum flooding surface (fig 4.1).

The deposition of a grey shale with alternating fine silt stone beds (ripple laminated, planer laminated) above this glaucony horizon suggests deposition was took place in a low energy marine environment and gradual deepening of depositional settings. The laterally persistent fine grained shale with abundance of pyrite deposit in an alternation of planer laminated fine siltstone bed(thick-thin) indicates suspension sedimentary fall out in a low energy environment. And this part define as anoxic offshore marine environment. So, the “alternating shale-fine silt stone sedimentary succession” was represented in a deeper marine environment than lower quartzite deposition. The presence of black shale in this association explains water level during deposition of black shale beds was higher compared to water level of Glaucony horizon deposition. So the sea level of this transgression system deposit emerge more earth surface exposure than lower sandstone deposit. The deposition of reworked volcanoclastic sediment (fine silt stone) in an alternation of shale bed also support more earth surface exposure emergence by sea level increase.

The gradual deposition of grey shale above “ Black shale with alternating planer laminated reworked volcanoclastic sedimentary deposit ” infer shallow water deposit compared to black shale with alternating planer laminated reworked volcanoclastic sedimentary deposit.

The presence of abundant blackshale above silt stone unit indicates low energy deeper shelf deposition. The intercalation of black shale and sandstone beds with hummocky cross stratification, gutter cast, flute and sole marks infer intervenetion of storm action in deeper shelf. The deposition of sand free pyritiferous black shale as top most sedimentary record represent the maxima of transgression (MFS).

Thus, we can represent the sedimentary record of lower part Kaimur formation as a transgressive system tract deposit. The transgressive lag in between the rohtas limestone and the sandstone unit above rohtas limestone represent the initiation of transgression. The presence of pyritiferous black shale as top most sedimentary record of lower part of kaimur sedimentary succession infer the maximum flooding surface of transgression. But the appearence of silt stone unit in between this transgressive system tract deposit infer temporary fall of relative sea level.

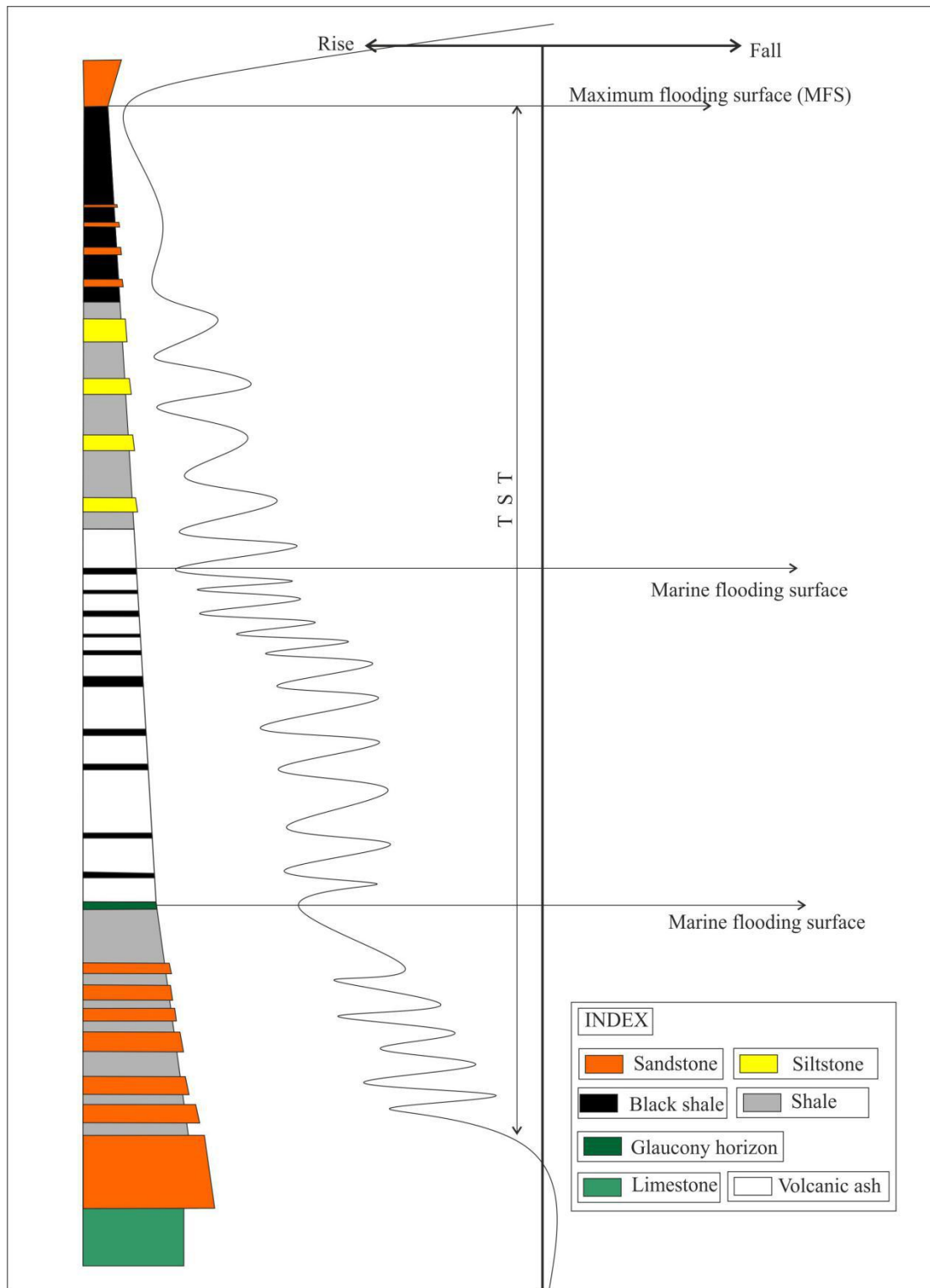


Fig. 4.1 Sequence stratigraphy representation during lower kaimur sediment deposition.

Chapter 5

Discussion and Conclusion

Discussion

The Rohtas Limestone, top most member of lower Vindhyan is overlain by a laterally persistent sandstone in study area. The sandstone initiated its deposition over a thin transgressive lag. The clasts of transgressive lag are consists of chertified limestone derived from Rohtas Limestone. It is likely that some parts of Rohtas Limestone were exposed for a long period of time which helps chertification (Kolodny et al., 1980). Transgressive lag at the base of sandstone deposition indicates a fresh sedimentation event after a long time period. The abundance of alternating thick-thin cross-stratification, herringbone cross-stratification, reactivation surfaces and double mud drape are the evidences of tide dominated environment. The presence of hummocky cross-stratification, conglomerate beds, massive beds with sharp erosional contact and sole marks indicates interruption of storm waves in a tide dominated depositional environment. Vertical transition of herringbone cross-stratification, alternating thick-thin cross-stratification to double mud drape from lower to upper part of the sandstone infer transition from intertidal to subtidal. Increasing shale thickness in vertical transition also supports sea level increment with time. The sandstone ceased its deposition with the appearance of a thick glaucony horizon.

The distribution of chemical composition in glaucony horizon infers glaucony is the “Fe illite”. The Fe-illite contains low TFe_2O_3 (4.50 to 9.60 wt %), high K_2O (6.69 to 8.27 wt %) and high MgO (2.18 to 3.85 wt %) which are exactly similar to the glaucony of Precambrian Vindhyan basin and other Precambrian in world as well. High MgO infer Precambrian ocean contains high Mg in sea water. Highly constant K_2O and replacement texture of feldspar infer glauconitization in feldspar grains. The cross plot of K_2O and TFe_2O_3 also supports replacement glauconitization model. The Fe^{2+} and Fe^{3+} ratio 0.8 and $\text{Fe}^{+2}/\text{TFe}$ 0.4 infer glauconitization in anoxic zone. The presence of both Fe^{3+} along with Fe^{2+} infers glauconitization within suboxic zone. The suboxic zone in Proterozoic time was above fair weather wave base. Glauconitization was occurred in a shallow subtidal environment with sub-oxic condition. The

glaucony horizon infer a condensed zone of transgressive system tract deposition i.e. a marine flooding surface.

The sandstone deposition vertically transit into an alternating silt-shale deposition. Silts are gray to dark gray in color, composed of reworked volcanoclastic sediments (Chakraborty, 2006). The shale is dark in colour. Within the dark shales plenty of microbial mat features are present. Abundance of pyrite grains along microbial mat layers infers reducing condition in the depositional site. Dominance of thick shale silt in depositional site infer high sea level during deposition. Deposition of black shale with some sand beds above siltstone infers deeper shelf deposition. Preservation of hummocky cross-stratification, sandstone with flute casts, sole marks infer intervention of storm surges during deposition. Again vertical transition to sand free thick black shale indicates maximum flooding surface.

Considering the sedimentological details of the Sandstone present above the Rohtas Limestone with an erosional surface in between, it is likely that the boundary between lower and upper Vindhyan must be placed below the sandstone unit and above the Rohtas limestone.

Conclusion

1. The unconformity between lower and upper Vindhyan in Son valley sector of the Vindhyan Supergroup lies between the Rohtas Limestone and the overlying sandstone which is stratigraphically equivalent to Sasaram sandstone (or Lower quartzite) .
2. The presence of Sasaram sandstone/ Lower Quartzite both in Bundelkhand and Son valley sector indicates initiation of a fresh sedimentation all over the Son valley after a gap in sedimentation.
3. Presence of transgressive lag containing chertified limestone calsts also supports the initiation of transgression.
4. Detailed study of the Sandstone indicate the deposition of the sediment took place in an intertidal to subtidal setting . This tide-influenced paleogeography was occasionally disturbed by storm events.
5. Tidal cyclicity, presence of double mud drape layer, herringbone-cross stratification confirm tidal influence.
6. Glaucony bed on top of Lower Quartzite represents condensates zone deposition in the transgressive system tract i.e. marine flooding surface.
7. High Mg in Lower Quartzite glaucony infers Mg rich Vindhyan Ocean.
8. The glaucony was formed in a shallow marine sub-oxic condition.
9. The glaucony was formed by replacement of feldspar grains.
10. The Bhagwar shale overlay the Lower Quartzite.
11. The presence of black shale in Bhagwar shale association infers deposition of Bhagwar Shale during the ongoing transgression and black part deposited during peak transgression [maximum flooding surface (MFS)]

References:

- A. Amorosi., The occurrence of glaucony in the stratigraphic record: Distribution patterns and sequence-stratigraphic significance. IAS Special publications (2013), pp. 37-53.
- Allen, J.R.L., 1980. Sandwaves: a model of origin and internal structure. *Sediment. Geol.*, 26: 281-328.
- Allen, J.R.L., 1982. *Sedimentary Structures, Their Characters and Physical Basis*, Vol. 1. Elsevier, Amsterdam, pp.459-463.
- Basu A, 1985. Reading provenance from detrital quartz; In: *Provenance of Arenites* (ed.) G G Zuffa (Reidel Publishing Co.) Pp. 231–247.
- B.D. Boornhold, P. Giresse., Glauconitic sediments on continental shelf off Vancouver Island , British Columbia, Canada. *Journal of Sedimentary Petrology* , 55(5) (1985), pp. 653-664.
- Bose, P.K., Chaudhuri, A.K., 1990. Tide versus storm in epiclastic coastal deposition: two Proterozoic Sequences. *Geol. J.* 25, 81-101.
- Bose, P.K., Sarkar, S., Chakrabarty, S., Banerjee, S., 2001. Overview of the Meso- to neoproterozoic evolution of the Vindhyan Basin, Central India. *Sedimentary Geology* 141-142, pp. 395-419.
- Chakrabarty, C., Bose, P.K., 1990. Internal Structure of sandwaves in a tide-storm interactive system: Proterozoic Lower Quartzite Formation, India. *Sediment. Geol.* 67, pp 133-142.
- Chakrabarty, P.P., Banerjee, S.S., Das, N.G., Sarkar, S., Bose, P.K., 1996. Volcaniclastics and their sedimentological bearing in Proterozoic Kaimur and Rewa groups in Central India. *Recent advances in Vindhyan geology*, Bhattacharya, A (Ed), *Geol. Soc. India, Mem.* 36, 59-76.
- Chanda, S.K. and Bhattacharya, A., 1982. Vindhyan sedimentation and paleogeography: post Aoudenberg developments. In: K.S. Valdiya, S.B. Bhatia and V.K. Gaur (Editors), *Geology of Vindhyan*. Hindustan Publishing Corporation. Delhi, pp. 88-101.

- Dalrymple, R.W., 1984. Morphology and internal structures of sandwaves in the Bay of Fundy. *Sedimentology*. 31: 365-382.
- Dickinson, W.R. and Suczek, C.A., 1979. Plate tectonics and sandstone compositions; *Am. Ass. Petroleum Geol. Bull.* 63, pp 2164-2182.
- G.S. Oudin, A. Matter., *De glauconiarum origine*. *Sedimentology*, 28(5) (1981), pp. 611-641. 214-229.
- D.J Tang, X. Y. Shi, J.B. Ma, G.Q. Jiang, X.Q. Zhou, Q. Shi., Formation of shallow-water glaucony in weakly oxygenated Precambrian ocean: An example from the Mesoproterozoic Tieling Formation in North China. *Precambrian Research*, 294 (Supplement C) (2017), pp
- H.S. Chafetz, A. Reid., Syndepositional shallow-water precipitation of glauconitic minerals. *Sedimentary Geology*, 136 (1-2) (2000), pp. 29-42.
- J. Afr. Earth. Sci. 30, 201-217. Gupta, K.D., Pickering K.T., 2008. Petrography and temporal changes in petrofacies of deep-marine Ainsa–Jaca basin sandstone systems, Early and Middle Eocene, Spanish Pyrenees. *Sedimentology* 55, 1083-1114.
- J.F. Burst “ Glauconite” pellets: Their mineral nature and applications to stratigraphic interpretations. *AAPG Bulletin*, 42 (2) (1958), pp. 310-327.
- J.F. Burst., Mineral heterogeneity in “ glauconite” pellets. *American Mineralogist*, 43(5) (1958), pp. 481-497
- Mazumder, R., Bose, P.K., Sarkar, S., 2000. A commentary on the tectono-sedimentological record of the pre-2.0 Ga continental growth of India vis-à-vis a possible
- Miall, A. D. 1985. Architectural-element analysis: a new method of facies analysis applied to fluvial deposits.
- Miall, A.D., 1991. Stratigraphic sequences and their chronostratigraphic correlation. *J. Sediment. Petrol.* 61, 497-505.
- Middleton, G. V., & Hampton, M. A. 1973. Part I. Sediment gravity flows: mechanics of flow and deposition.
- Reading, H.G., 1996. *Sedimentary Environments: Processes, Facies and Stratigraphy*. Blackwell Science, pp. 688.
- S. Banerjee, S. Mandal, P.P. Chakraborty, S.S. Meena., Distinctive compositional characteristics and evolutionary trend of Precambrian

glaucy: Example from Bhalukona Formation, Chattisgarh Basin, India. *Precambrian Research*, 271 (2015), pp. 33-48.

- S. Banerjee, U. Bansal, A.V. Thorat., A review on palaeogeographic implications and temporal variation in glaucy composition. *Journal of Palaeogeography*, 5(1) (2016), pp. 43-71.
- S. Banerjee, S. Jeevankumar, P.G.Eriksson., Mg- rich ferric illite in marine transgressive and highstand system tracts: Examples from the Paleoproterozoic Semri Group, central India. *Precambrian Research*, 162 (1-2) (2008), pp. 212-226.
- S.Dasgupta,A.K Chaudhuri,M. Fukuoka., Compositional characteristics of glauconitic alterations of K-feldspar from India and their implications. *Journal of Sedimentary Petrology*, 60(2) (1990), pp. 277-281
- Singh, I.B., 1973. Depositional Environments of the upper Vindhyan Sediments in Son Valley area. In: Valdiya, K.S., Bhatia, S.B., Gour, V.K., (Eds.), *Geology of Vindhyan*. Hindustan Publishing (India), Delhi, pp. 146-152.
- S.S. Chanh, Y.H. Sahu, M.K. Wang, C.T. Ku, P.N. Chiang., Mineralogy and occurrence of glauconite in central Taiwan. *Applied Clay Science*, 42(1) (2008), pp. 74-80.
- U. Bansal, S. Banerjee, K. Pande, A. Arora, S.s. Meena., The distinctive compositional evolution of glauconite in the cretaceous Ukra Hill Member (Kuch basin, India) and its implications. *Marine and Petroleum Geology*, 82 (2017), pp. 97-117.
- Walker, R.G., 1984. Facies Models. Geological Association of the Canada, New foundland, Canada, pp 317.
- Venkatachala, B.S., Sharma, M., Shukla, M., 1996. Age and life of Vindhyan: Facts and conjectures. Recent advances in Vindhyan Geology, Bhattacharya, A. (Ed.), *Geol. Soc. India Mem.* 36, 137-166.
- Walker, R. G., 1984. Turbidites and associated coarse clastic deposits. In: Walker, R. G., (Ed). *Facies Models* (second edition). Toronto: Geological Association of Canada, 171- 188.